SOLAR ACTIVITY AND GEOMAGNETIC STORM EFFECTS ON GPS IONOSPHERIC TEC OVER ETHIOPIA

By

Aragaw Msganaw

SUBMITTED IN PARTIAL FULFILLMENT OF THE
REQUIREMENTS FOR THE DEGREE OF
MASTER OF SCIENCE IN PHYSICS (SPACE PHYSICS)
AT
ADDIS ABABA UNIVERSITY
ADDIS ABABA, ETHIOPIA
AUGUST 2017

ADDIS ABABA UNIVERSITY
DEPARTMENT OF
PHYSICS

The undersigned hereby certify that they have read and recommend to the Faculty of Natural and Computational Science for acceptance a thesis entitled "**Solar activity and geomagnetic storm effects on GPS ionospheric TEC over Ethiopia**" by **Aragaw Msganaw** in partial fulfillment of the requirements for the degree of **Master of Science in Physics (Space Physics)**.

Dated: August 2017

Examiner: _____
Dr. Tilahun Tesfaye

Examiner: _____
Dr. Teshome Senbeta

Advisor: _____
Dr. Gebregiorgis Abraha

Chairman: _____
Dr. Deribe Hirpo

ADDIS ABABA UNIVERSITY

Date: **August 2017**

Author: **Aragaw Msganaw**

Title: **Solar activity and geomagnetic storm effects on GPS ionospheric TEC over Ethiopia**

Department: **Physics**

Degree: **MSc.** Convocation: **September** Year: **2017**

Permission is herewith granted to Addis Ababa University to circulate and to have copied for non-commercial purposes, at its discretion, the above title upon the request of individuals or institutions.

Signature of Author

Table of Contents

List of Figures

Abstract

Ionospheric GPS total electron content (TEC) is an important parameter to monitor for possible Space Weather impacts. The effects of solar activity on TEC at low latitude stations with geographic locations (latitude, longitude) of Addis Ababa (9.04^0 *N,* 38.77^0 *E) and Bahir Dar (*11.6^0 *N,* 37.36^0 *E) in Ethiopia, East Africa in the year of 2015 around peak of solar cycle 24 has been carried out. The data from the two stations were used to study the diurnal, monthly and seasonal variations of TEC and its dependence with solar activity and space weather effects. The results of the analysis reveal that TEC undergoes diurnal and seasonal variations. From the daily variation analysis, the TEC value at both stations sharply increases to its peak value from* $0900 - 1500$ *UT and decreases around* $1600 - 0700$ *UT. Seasonal variations showed that TEC maximizes during the equinoctial months and least in summer, over the two stations. In all seasons the maximum value of TEC leads first in Addis Ababa. These observations were investigated and further discussed with an analysis of Disturbance Storm Time (Dst) and Ap indices, solar radio flux (F10.7 cm) and sunspot number during the period of 2015. During the period of low or high sunspot number, the provided GPS ionospheric TEC builds up slowly or quickly. As a typical case of storm-time behavior, a geomagnetic storm of June 23, 2015 is considered in this study. The Dst values for the period shows that it is an intense intensity geomagnetic storm. The effects of geomagnetic storms on TEC values have been found negative and positive output.*

Keywords: Solar activity, GPS, Ionosphere, TEC, Geomagnetic storm, Ethiopia.

Acknowledgements

At the very onset, I surrender myself before the Almighty God with his mother saint Mariam for blessing me with the best of what I could have had. Really, I was in serious health problem during organization of this thesis if saint water of saint Mariam's church found at Addis Ababa was not treated me. I deeply appreciate my supervisor Dr. Gebregiorgis Abraha for the strong academic supervision, guidance and intelligent suggestions he provided throughout the research period. His vast knowledge and experience in science will always remain with me as an example to follow. I would like to record my words of thanks to Dr. Tsegaye Kassa for his support and initiation to use GPS TEC data and having short but healthy discussions on the course and ways of the research work with his staff members Ambelu and Habitish. My sincere thanks goes to Abera Debebe (my under graduate instructor and PhD candidate) for his support on a breakthrough knowledge on MATLAB which has indispensable role to do my thesis. I am highly indebted with Dr. Teshome Senbeta and Dr. Belayneh Mesfin, the current and former physics Department heads, for specialization chance they gave me. This thanks goes to physics department as a whole. I am also very grateful to all my remedial and masters lecturers for their enthusiastic imparting baseline knowledge. Special thanks to Getachew Bayeh a means to join this field, Birara Tilahun for his undenied call help, Ephrem and w/ro Tsilat Adnew for kind cooperation. I am grateful to acknowledge Addis Ababa University and MOE for the research fund and the chance respectively, WDC, UNAVCO and Omniweb, the authors of research journals publications and books. I bow innovation to my lovely wife (Genet Geta) and my son (Natinael Aragaw) for their care and kindness. My words of thanks cannot compensate their contribution, all humility I thank them for their noble gesture and splendid support. Finally, I would like to express my thanks to all my family members and friends for their love and support.

Chapter 1

Introduction

Space Science and Technology is becoming one of the critical and fundamental pillar of sustainable development in the world and Ethiopia should not be left out in this all important technology. The Sun's violent activity and many unexpected and unpredictable events taking place on its surface suggest that we should prepare for the worst. As mankind has become increasingly dependent on technology, understanding of the effects of the Space Physics phenomena on human technology, termed Space Weather, has become increasingly necessary. It is concerned with conditions within the solar system which are driven by variable solar activity. The Sun is the source of normal terrestrial weather [1].

The changes on the Sun cause effects in space, in the atmosphere, and on Earth's surface. Most aspects of Space Weather affect us to some extent. The more our society becomes dependent on technology and the more we utilize space, the more we are affected by Space Weather. Its effects are highly relevant to our daily life on Earth. Technology dependence has become increasingly vulnerable to adverse Space Weather. Topics such as crew and passenger radiation risks on aircraft, communication problems, effects on GPS and satellite systems, can be directly linked to Space

Weather. Even power-lines failures and corrosion effects observed in pipelines on Earth may be the direct result of Space Weather induced effects and should be taken very seriously [2, 3].

Huge explosions of magnetic field and plasma from the Sun's corona, known as coronal mass ejections (CMEs), could one day produce extremely powerful geomagnetic storms striking Earth with enormous power, showing no mercy to our planet. CMEs are the most dangerous and destructive Space Weather events. When the Sun produces CMEs that travel to the Earth they can carry magnetic field of opposite polarity to that of the Earth. This in combination with a solar wind enhanced by the CME weakens the Earth's magnetic field allowing energy to reach the Earth. This creates rapid changes in the Earth's magnetic field causing a strong magnetic storm [4].

Geomagnetic storm is a worldwide disturbance of the Earth's magnetic field, associated with solar activity. The solar wind fills the solar system and the Earth is constantly bombarded by this steady flow of particles and magnetic field. These magnetic storms induce currents on the ground in power grids, pipelines, railway signaling and magnetic fluctuations that affect surveying and drilling for oil and gas.

The real long-lasting danger comes from the storm's effect on technology. The flurry of magnetic activity and induced electric currents has the potential to severely disrupt power grids, satellites, communication networks-anything that uses electricity.

Due to the largest storm recorded ever before (Carrington Event, after amateur astronomer Richard Carrington who observed the flares that triggered the storm, 1859), six million people were without power for nine hours. Cascading failures could quickly shut-power down to millions of people in a matter of minutes. Communication

networks would fail and GPS satellites, upon which the entire air traffic system relies, would shut down. A repeat of the Carrington Event in today's far more interconnected world would be devastating. That's why Astronomers study the Sun [5, 6].

Besides the joy of discovering how stars work, a better understanding of solar activity can help us be better prepared. With even just a few hours warning before an impending CME strike, we could safely shut-down and protect essential services. Disruptions may then only last a few hours, rather than the days, weeks, and months that might otherwise occur.

Another consequence of magnetic storms is heating of the upper atmosphere. This changes the density in the ionosphere disrupting radio signals, in particular satellite navigation systems. The solar plasma impact on Earth's magnetosphere resulting in geomagnetic storms originates from two sources on the Sun: the coronal mass ejections (CMEs) from closed magnetic field regions and high speed solar wind streams (HSS) from coronal holes, which are open magnetic field regions. When a CME or high speed stream arrives at Earth it buffets the magnetosphere [2].

If the arriving solar magnetic field is directed southward it interacts strongly with the oppositely oriented magnetic field of the Earth. The Earth's magnetic field is then peeled open like an onion allowing energetic solar wind particles to stream down the field lines to hit the atmosphere over the poles [7, 8].

The study of these worldwide disturbances of Earth's magnetic field are important in understanding the dynamics of solar-terrestrial environment. Although the technology was affected only by the most severe ones in the past, nowadays our society demands more sophisticated technology, therefore may become more vulnerable even at less severe disturbances. Methods for forecasting Space Weather have thus

generated considerable research interest. For the ground-based applications, the geomagnetic activity is the key manifestation of Space Weather [9, 10, 11].

The long term variability in the geomagnetic activity has several sources. For instance, the variability of the Sun itself that is reflected on the solar wind causes the 11 and 22−year solar cycles, while the rotation of the Sun around its axis produces a periodicity of 27 days. The level of geomagnetic activity is measured using different activity indices, such as Dst, Ap and AE, most of which are derived from ground based magnetic field measurements. The indices are also often used to bin observation with respect to the level of geomagnetic activity.

From the terrestrial perspective, Space Weather is associated especially with the Earth's magnetosphere [12]. The processes in the magnetosphere have their consequences in the ionosphere and in the variations of the geomagnetic field, which can be observed at ground-based magnetic observatories. The causal connection between the solar activity and the geomagnetic activity has been reproved many times. Many phenomena of this causal chain have been understood in detail; however, reliable methods for forecasting magnetic storms still remain difficult to reach [13] for some model statistics and ranking.

The atmosphere still provides enough protection for everyone on the ground. The atmosphere of Earth is a layer of gases surrounding the planet Earth that is retained by Earth's gravity. It protects life on Earth by absorbing ultraviolet solar radiation, warming the surface through heat retention, and reducing temperature extremes between day and night (the diurnal temperature variation). A region of partially ionized plasma above the Earth's atmosphere formed due to primarily photo-ionization of the

neutral atoms and molecules that affect radio wave propagation is termed as ionosphere [2, 5, 6].

The increase in the density of the atmosphere as we go further down to the surface of the Earth and the decrease in the intensity of photons as it bombards the neutral atoms and the availability of different atoms and molecules at different heights from the Earth's surface forms a large scale vertical layer of ionization within the ionosphere. This makes the ionosphere to exist as vertically stratified partially ionized plasma state from at about $60 - 1000$ km from the surface of the Earth [8]. The electron density distribution over this region is, therefore, very crucial for satellite communication and navigation systems. However, the distribution of these electrons over the ionosphere exhibits complicated structure especially during increased solar activity. Hence, exploring the ionosphere is of utmost interest due to the complexities associated with the region [9, 10, 14].

One of the parameters that can be used to study the ionosphere is the Total Electron Content (TEC). The variability of the ionosphere can be monitored using space and ground based probing techniques. Among the different techniques, the global positioning system (GPS), which uses a linear combination of observable two frequencies to remove the effect for positioning is used in this study.

Due to insufficient ionospheric devices the physics of the ionosphere in Ethiopia has not been studied well. Now a days few ground based GPS receivers have been installed and as a result it gives a good opportunity for us to observe effects of solar activities on GPS ionospheric TEC. The computation of reliable vertical total electron content (VTEC) of the ionosphere is at the same time an useful and challenging goal. Useful because, in both Science and Technology fields, they can provide valuable

information concerning Space Weather Events, empirical model predictions, and user navigation improvement, among others [15, 16].

Because of the sensitivity of the science as stated above and the insufficient studies about ionospheric variability in Ethiopia, East Africa, we are motivated to observe the effects of solar activities and geomagnetic storms by using ground based GPS receivers over this country with recent data.

The main objective of this study is thus, to investigate effects of solar activities and geomagnetic storms on GPS ionospheric TEC over Ethiopia by using Addis Ababa and Bahir Dar GPS stations in the year of 2015, around peak of solar cycle 24.

This study is organized by six chapters: Chapter 1 presents introduction including organization of the study, Chapter 2 deals about Space Weather, the Sun and its activity. In Chapter 3 the Earth's atmosphere and ionosphere, atmospheric regions based on temperature profile, ionospheric variabilities and its disturbances are described. Chapter 4 briefs data and methodologies used. Chapter 5 presents results and discussions in terms of diurnal, monthly and seasonal variation of TEC as consequences of the solar activities change in line with sunspot number, solar radio flux and its variability due to Space Weather Events. Chapter 6 presents conclusions and recommendations of the study respectively.

Chapter 2

Space Weather

2.1 What is the need to study ionosphere?

The rapidly varying ionospheric currents cause rapid time variation in the magnetic field on the surface of the Earth as well as on the upper atmosphere at different levels. The change in geomagnetic field in turn induces a current according to Faraday's law and is given by: $\frac{\partial \vec{B}}{\partial t} = - \bigtriangledown \times \vec{E}$. When these currents flow in man made conductive networks they are called magnetically induced currents and these induction effects can felt in gas pipelines buried underground and under sea telecommunication cables power grids and can damage these systems [3, 17].

We can imagine our world with out electricity, the society depends on electricity for everything such as communication, banking and business transaction to basic necessities like food and water. One serious fact to the reliability of electric power is geomagnetic storm, which induces huge current fluctuation in the upper atmosphere. This current induces magnetic flied in the surrounding space and this in turn modifies the intensity of the magnetic field of the Earth. This modification by itself is resulted in producing additional current to trigger voltage fluctuation in transformers [17].

The other important thing we need to study the ionosphere is because it affects

modern technologies such as civilian and military communications, navigation systems and surveillance systems, etc. For many communication and navigation systems, this arises because the systems use signals transmitted to and from satellites, which must therefore pass through the ionosphere. For the most reliable communication and navigation it is necessary to correct the signals for effects imposed by the ionosphere. To do that the properties of the ionosphere, such as its variability with respect to magnetospheric disturbance, time of day, season of the year, and solar cycle variability must be well understood using different observing techniques. Radio wave propagation is modified in a number of ways by the effects of the integrated electron density along the ionospheric ray path between the satellite and the receiver, the TEC [10, 17].

In consequence, TEC is a key parameter in the description of the impact of the ionized atmosphere on the propagation of radio signals. Therefore, understanding the variability of TEC is crucial for the operation of many applications, including navigation satellite systems like Global Positioning System (GPS) and Global Navigation Satellite System (GLONASS). TEC can be measured by a number of essentially standard techniques, including Faraday rotation, group delay, and dispersive carrier phase. The TEC estimation technique from GPS satellite signal group delay and dispersive carrier phase advance is the popularly used method. Therefore, using data from both ground-based GPS receivers and the GPS receivers on Low Earth Orbit (LEO) satellites, GPS-TEC measurements become one of the best for observing the entire vertical extent of the ionosphere (i.e. both the bottomside and topside ionosphere), especially for correcting satellite navigation systems [17].

2.2 General about the Sun

The Sun is a huge gaseous globe situated at the center of the solar system, like a star and with an effective temperature of about 5800 K. It is almost perfectly spherical, having a diameter of about $1,392,684$ km around 10^9 times that of Earth and its mass is 1.989×10^{30} kilograms, (approximately 330,000 times the mass of Earth) which accounts for about 99.86 of the total mass of the Solar System. Sun is the typical star that generates energy due nuclear fusion. The Sun's gravity is by far the most powerful force in the solar system strong enough to hold all of the planets and comets in orbit. In fact, 99.8% of the mass of the solar system is in the Sun. The Sun is the heart of the solar system. Like Earth, the Sun has an interior and an atmosphere. Occasionally a huge release of magnetic energy, called a solar flare, occurs on the Sun. Flares can produce large quantities of x-rays which affect the Earth's atmosphere. They can also accelerate atomic particles (mostly protons) to very high speeds (a substantial fraction of the speed of light!). These high energy particles are dangerous to man and can reach the stratosphere where jet aircraft fly [18].

2.2.1 The Sun's interior

The interior structure of the Sun is classified in to core, radiation zone and convection zone due to their temperature, density and the property of the energy as shown in Fig. 2.1.

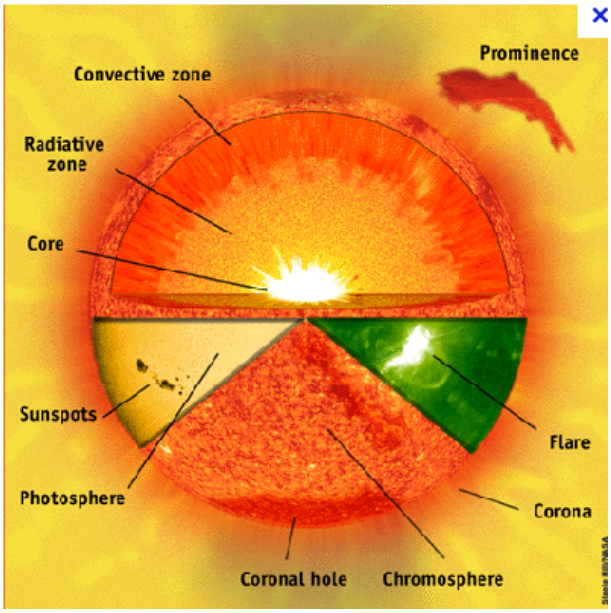

Figure 2.1: The layers and atmosphere of the Sun.

2.2.2 The Sun's atmosphere

The atmosphere of the Sun is composed of several layers, mainly the photosphere, the chromosphere and the corona. It's in these outer layers that the Sun's energy, which has bubbled up from the Sun's interior layers, is detected as sunlight. There are no boundaries between the layers of the Sun.

The Photosphere

The lowest layer of the Sun's atmosphere is the photosphere. It is about 300 miles (500 kilometers) thick. This layer is where the Sun's energy is released as light. Because of the distance from the Sun to Earth, light reaches our planet in about eight minutes. The inner most region reaching out to about 500 km above the top of the convection zone is the photosphere. The photosphere is a very thin, cool layer from which the visible light (radiation) is emitted. In the photosphere the temperature (T) as well

as the density (ρ) decreases. The light of the Sun comes from the photosphere, which has a temperature of about 5800 K [1].

The Chromosphere

The Greek word chromo means color, so chromosphere is the color sphere. The temperature of the Sun rises to about $10,000$ K in the chromosphere and it extends about 2×10^3 km from the photosphere. During a total solar eclipse the moon blocks light from the photosphere. At the beginning and end of a total eclipse, you can see a reddish glow just around the photosphere (visible during solar eclipses). This glow comes from the middle layer of the Sun's atmosphere, is called the chromosphere. Above the photosphere the temperature passes through a minimum of 4000 K and then rises to several 10^4 K in the chromosphere and much more rapidly in the transition region until the coronal temperature (10^6 K) is reached [1].

The corona

The corona that extends 10^6 km out into space from the chromosphere. In the middle of a total solar eclipse, the moon also blocks light from the chromosphere. At these times an even fainter layer of the Sun becomes visible. This outer layer, which looks like a white halo around the Sun, is called the corona, which means crown in Latin. From Earth's surface, the corona is only visible during eclipses or from special telescopes. But Astronomers can use telescopes in space to observe the corona all the time and to study how it changes. The corona sends out a stream of electrically charged particles called solar wind. The corona is further away from the center of the Sun than photosphere and chromosphere. But the temperature in corona is about 2 million degree kelvin at the base of corona and remains that hot as

it reaches the Earth. One hypothesis says that the coronas temperature results from the effects of magnetic fields instead of radiation from the Sun's core. Intense and strong magnetic loops exist in corona. Because of the Sun's rotation these magnetic loops store magnetic energy and when they interact they release their stored energy into corona providing the energy that keeps corona so hot [1, 18].

2.2.3 Different features of the Sun

For hundreds of years scientists have used telescopes to look at the Sun. Features on or above the Sun's surface include sunspots, prominence, solar flares and the like.

Solar flares

It is a sudden, rapid and intense variation in brightness on the Sun. It occurs when magnetic energy that has built up in the solar atmosphere is suddenly released due to reconnection of magnetic fields. Solar flares can greatly increase the solar wind from the corona, resulting in an increase in the number of particles reaching Earth's atmosphere. These solar wind particles can affect Earth's upper atmosphere, causing magnetic storms [19].

Prominence

Another kind of solar explosion stems from a prominence (reddish loops of gas called prominence link different parts of sunspot regions). The prominence extends far into the Sun's upper atmosphere and follows the loop of a closed magnetic flux tube, with the ends of the loop rooted in sunspots. A prominence is a huge, looping mass of gas seen above the chromosphere.

Sunspots

Sunspots are temporary phenomena on the photosphere of the Sun that appear as dark spots compared to surrounding regions. They are areas of reduced surface temperature caused by concentrations of magnetic field flux that inhibit convection. Sunspots usually appear in pairs of opposite magnetic polarity [20]. Their number varies according to the approximately 11-year solar cycle. Individual sunspots may endure anywhere from a few days to a few months, but eventually decay. Sunspots expand and contract as they move across the surface of the Sun with sizes ranging from 16 kilometers (10 mi) [21] to 160,000 kilometers (100,000 mi) in diameter. The larger variety are visible from Earth without the aid of a telescope. They may travel at relative speeds, or proper motions of a few hundred meters per second when they first emerge. Indicating intense magnetic activity, sunspots accompany secondary phenomena such as coronal loops (prominence) and reconnection events. Most solar flares and coronal mass ejections originate in magnetically active regions around visible sunspot groupings. Similar phenomena indirectly observed on stars other than the Sun are commonly called starspots and both light and dark spots have been measured [19, 20, 21].

Coronal Mass Ejections

Coronal mass ejections (CMEs) are tremendous amount of bubbles of electrified gas that streaming away from the Sun. They can carry as much as 10 billion tons of solar material and usually travel at speeds between 500 and 1500 km/s, taking 2 or 3 days to cross the 150 million km which is the distance between Sun and Earth. The occurrence rate of CMEs increases during the maximum of the solar activity cycle [22].

An Earth-directed coronal mass ejection will look like a partial or full-halo coronal mass ejection on the images from Solar and Heliospheric Observatory (SOHO). When this happens the coronal mass ejection will arrive at Earth after 24 hours or more (depending on the speed) and will likely cause a geomagnetic storm with vivid auroral displays. The animation shown in Fig 2.2 is a full-halo coronal mass ejection as seen by Solar and Heliospheric Observatory/Large Angle and Spectrometric Coronograph (SOHO/LASCO) when billion tons of plasma launched two million kilometers off the surface of the sun!. The dark area in the middle of the image is from a disk used to block out the light of the Sun. The white circle outlines the location of the Sun's surface.

Fast CMEs, those which outpace the ambient solar wind, give rise to large geomagnetic storms when they encounter the Earth's magnetosphere [23]. Such storms can result from the passage either of the CME itself or of the shock created by the fast CME's interaction with the lower-moving solar wind.

Geomagnetic activity associated with CMEs can dramatically disrupt electrical and communications systems. CMEs can create voltage surges in electric power grids, disrupt radio communications and navigation systems, prevent normal satellite operations, and threaten the safety of astronauts [3, 24]. In 1997, for example, a geomagnetic storm shut down a satellite that provided television broadcasts. In 1998 another storm disrupted a Galaxy IV satellite that supported automated cash machines and airline tracking systems. Geomagnetic storms are also known to affect mobile phone operations and wireless internet services.

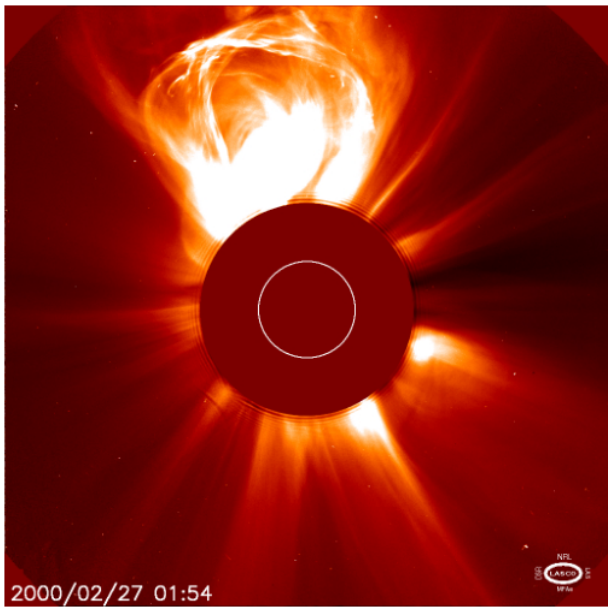

Figure 2.2: CME recorded by the SOHO satellite in 2000. Taken from: (*https* : *//www.spaceweatherlive.com/en/help/what − is − a − coronal − mass − ejection − cme.*)

Solar wind

For many applications, interplanetary space can be considered a perfect vacuum. But the environment surrounding the Sun contains a flow, of mostly charged particles (electrons, protons and ions), with about 3% of α-particles and smaller amounts of multiply ionized heavier elements known as the solar wind. The gravity of the Sun is not strong enough to maintain static equilibrium in the solar corona, which continuously expands outwards into the interplanetary space as the solar wind. The solar wind is a plasma of charged particles coming out of the Sun in all directions at very high speeds ($250 - 1000$ km/s, i.e., about $600,000 - 2,000,000$ miles/hour). It varies with the changing conditions on the Sun. The solar wind is very hot, with typical temperatures of the order of 1 million K, but extremely diluted, with only a

few particles per cubic centimeter [3, 23, 24].

Magnetosphere

The region above the Earth's ionosphere in which the magnetic field of the Earth has a dominant control over the charged particles from the solar wind is called magnetosphere. The interaction of charged particles with the Earth's magnetic field compresses the field lines on the day side and stretching them out on the night side. The boundary separating the magnetosphere from the solar wind is called the magnetopause. In the classical and simplified schema of the magnetosphere, the charged particles composing the solar wind start to interact with the lines of the geomagnetic field on the dayside direction producing a shock wave, known as a bow shock for its shape, which could be considered as the border of the circum terrestrial region as shown in Fig 2.3. This bow shock separates the undisturbed solar wind from the shocked flow. On the Sun-Earth line, the bow shock is located at the distance of about 13 Earth radii ($RE = 6371.2$ km) from the centre of the Earth.

2.3 Solar energy from the Sun to Earth's surface

Nearly all the energy in Earth's atmosphere comes from the Sun. Sun burns are caused by ultraviolet radiation. This radiation can also cause skin cancer and eye damage. Before the Sun's rays can reach Earth's surface, they must pass through the atmosphere. Some of the energy from the Sun is absorbed within the atmosphere, water vapor and carbon dioxide absorb some infrared radiation. The ozone layer on the stratosphere absorbs most of the ultraviolet radiation. Clouds and other gases also absorb energy from the Sun. Some of the Sun's rays are reflected. Clouds in the

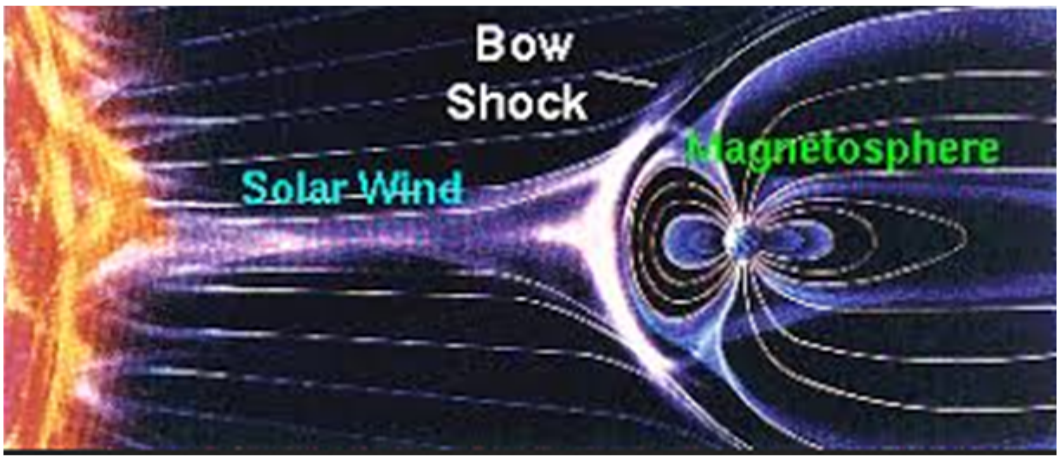

Figure 2.3: The solar wind interaction with the Earth's magnetosphere. Taken from: (*https : //www.google.com/search?q = solar + wind + magnetosphere + coupling.*)

atmosphere act like mirrors, reflecting some solar energy back into space. In addition particles and molecules of gases in the atmosphere reflect light from the Sun in all directions. Some of the Sun's energy reaches Earth's surface and is reflected back into the atmosphere. Some of the energy, however, is absorbed by the land and water and changed into heat. When Earth's surface is heated, it radiates some of the energy back into the atmosphere as infrared radiation. This infrared radiation can not travel all the way through the atmosphere back into space. Instead, much of it is absorbed by water vapor, carbon dioxide, methane, and other gases in the air [19, 25].

2.4 Space Weather Effects

The dynamic processes associated with the solar wind-magnetosphere-ionosphere coupling processes can have significant effects in the near-Earth space environment, in the atmosphere, and on the Earth's surface. As our lives have become increasingly dependent on technological systems that are vulnerable to electromagnetic disturbances

and bombardment by energetic electrons and ions, understanding these processes is important both for the design and maintenance of these systems. Space Weather Effects are highly relevant to our daily life on Earth. Technology dependence has become increasingly vulnerable to adverse Space Weather as shown in Fig. 2.4. Topics such as crew and passenger radiation risks on aircraft, communication problems, effects on GPS and satellite systems, can be directly linked to Space Weather. Even power-lines failures and corrosion effects observed in pipelines on Earth may be the direct result of Space Weather induced effects and should be taken very seriously [1, 3].

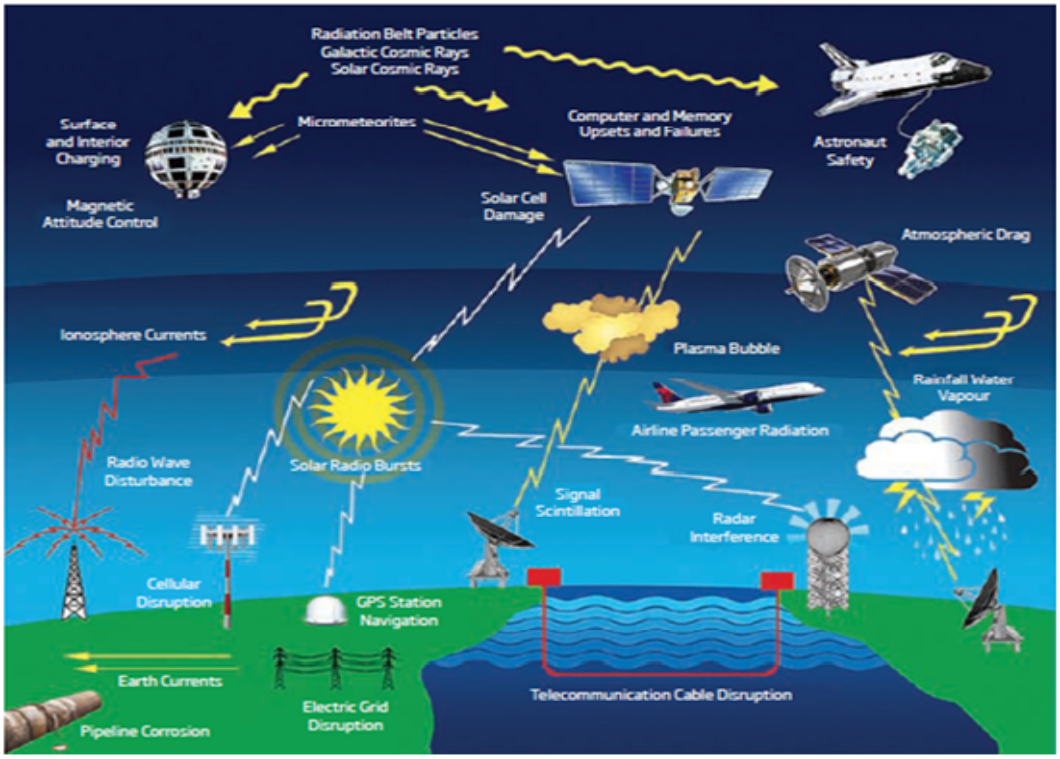

Figure 2.4: Space Weather Effects. Taken from: ($https://www.google.com/search?q=space+weather+effects.$)

2.5 Earth's Space Environment

Our reliance on technological systems, such as spacecraft missions, power systems, navigation systems and communications, is growing, and these systems are shown to be vulnerable to the unpredictability of Space Weather conditions. In fact, the risks for disruption of satellite operations, communications and power grids on the ground could be minimized if reliable forecasts of Space Weather were possible. Studies have already begun aimed at predicting the sequence of extreme conditions that occur in the solar-terrestrial coupling system. Space Weather plays an ever-increasing role in our society as human beings develop more and more delicate technologies in space and on Earth. In view of the crucial effects of geomagnetic storms on such human societal systems as radio communications and satellite drag, there is a strong need for prediction schemes to be continually upgraded. It is essential to integrate our observation and modeling efforts in the Space Weather Project [8].

Chapter 3

The Earth's Atmosphere and Ionosphere

3.1 The Earth's Atmosphere

The layer of gas around the solid Earth provides the oxygen we breath, protects us from ultraviolet radiation from the Sun, and acts as insulation to prevent extreme temperature swing from the day to night. Our benign atmosphere is unique in the solar system [14, 26].

3.1.1 Composition of the Earth's Atmosphere

Near the surface, the Earth's atmosphere contains about 78% nitrogen, 21% oxygen, 1% argon, and traces of water vapor, carbon dioxide, and many other gases. Although nitrogen and oxygen predominate throughout the atmosphere, the atomic and molecular makeup of the atmosphere changes with latitude [14].

3.1.2 Thermal Structure of the Earth's Atmosphere

Although density and pressure fall steadily with altitude, temperature does not. Temperature alternatively decreases and increases with height. In general layers of the

Earth's atmosphere are warm if they contain gases that absorb Sun light. Transparent layers (pauses) are cool [26, 27]. The layers of the Earth's atmosphere due to temperature are listed as below:-

Troposphere

It is the lowest region of the Earth's atmosphere where most of the gases appear. On average, it extends from the ground to an altitude of about 10 km. The ground absorbs sunlight and heats the air that is in contact with it. This heating plus the absorption of infrared solar radiation by water vapor, is concentrated in the lower troposphere. The rate of heating falls swiftly with altitude and so does temperature. Near the ground, the temperature drops by 6.5 k for every kilometer of increasing altitude. Whenever temperature decreases rapidly with altitude, convection occurs, as it does in the troposphere. The drop of temperature with height gradually becomes less steep until, at the tropopause, it becomes so small that convection ceases. Tropopause is the boundary of troposphere and stratosphere and it is a very coldest region with about 200 k ($-100\ ^0F$) [15, 28].

Stratosphere

It extends from the tropopause up to about 30 km. Ozone (O_3) layer located between $15 - 40$ km above ground, absorb a large portion of solar radiation between 200 and 300 km. Due to the presence of (O_3) temperature increases with height in this region. In the lower stratosphere there are often high-speed winds known as the jet stream [15, 29].

Mesosphere

It is a region where heating by absorption of solar radiation occurs. Ultraviolet radiation is absorbed by oxygen molecules, which are broken up in to atomic oxygen. The oxygen atoms react with other oxygen to produce ozone, which is effective at absorbing solar Ultraviolet radiation. The absorption of solar radiation by ozone heats the region from 30 to 60 km. The heating is greatest and temperature is highest, at about 50 km, where the temperature is about 300 k (about the same as the temperature at the ground). Although heating is greatest in the mesosphere, the ozone layer extends downward in the stratosphere as well. The ability of the ozone layer to block potentially lethal solar Ultraviolet radiation is vital to the continued existence of life on the Earth. Because of ozone abundance falls steeply above 50 km, heating becomes less effective and temperature drops until it reaches a minimum of about 180 k ($-135\ ^0F$) at about 90 km. This region is the mesopause [29].

Thermosphere

In the thermosphere, temperature climbs steadily, mostly because of the absorption of Ultraviolet (UV) radiation by nitrogen and oxygen atoms. The solar radiation that heats the thermosphere is relatively short-wave length UV radiation, which is completely absorbed in the thermosphere and does not survive to heat the lower atmosphere [15, 29]. Graphically the Earth's atmosphere is represented as shown in Fig. 3.1.

Exosphere

The exosphere is the most distant atmospheric region from Earth's surface. In the exosphere, an upward traveling molecule can escape to space (if it is moving fast

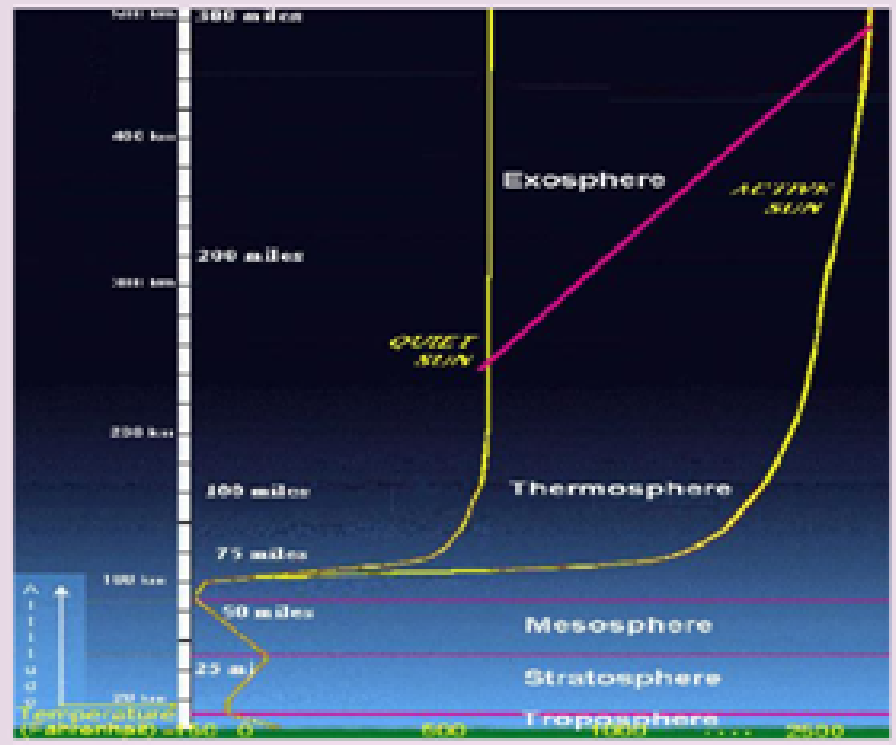

Figure 3.1: The temperature profile of the Earth's atmosphere. Taken from: (*https* : *//www.google.com/search?biw.*)

enough) or be pulled back to Earth by gravity (if it isn't) with little probability of colliding with another molecule. The altitude of its lower boundary, known as the thermopause or exobase, ranges from about 150 to 300 miles ($250 - 500$ km depending on solar activity. The upper boundary can be defined theoretically by the altitude (about $120,000$ miles, half the distance to the Moon) at which the influence of solar radiation pressure on atomic hydrogen velocities exceeds that of the Earth's gravitational pull. The exosphere observable from space as the geocorona is seen to extend to at least $60,000$ miles from the surface of the Earth. The exosphere is a transitional zone between Earth's atmosphere and interplanetary space [2].

3.2 The Earth's Ionosphere

In a region extending from a height of about 50 km to over 600 km, some of the molecules of the atmosphere are ionized by radiation from the Sun to produce an ionized gas. This region is called the ionosphere. Ionosphere is the region of the upper atmosphere where free electrons occur in sufficient density to have an influence on the propagation of radio frequency electromagnetic waves. Its ionization mostly depends on activity of the Sun. Its density varies according to the sunspot cycle, the season, and global locations polar, auroral zones, mid-latitudes, and equatorial regions. Most of its ionization is produced by x-ray and UV radiation from the Sun. As Earth rotates, ionization increases in the sunlit atmosphere and decreases on the shadowed side. The ionospheric electron density N at a given altitude and location depends on the solar EUV fluxes, the neutral composition, and dynamical effects of neutral winds and electric fields [30].

3.2.1 Vertical Profile of the ionosphere

The vertical structure of the ionosphere is changing continually. It varies from day to night, with the seasons of the year, and with altitude. In terms of altitude, the ionosphere may be subdivided into a number of different regions. These regions known as the D, E, F1 and F2 are formed by their chemical components and their ability to absorb different wavelengths of radiation emitted from the Sun, which causes a heterogeneous spread of ions and electrons in the upper atmosphere [30]. The general characteristics of the layers are expressed as observed from Fig. 3.2.

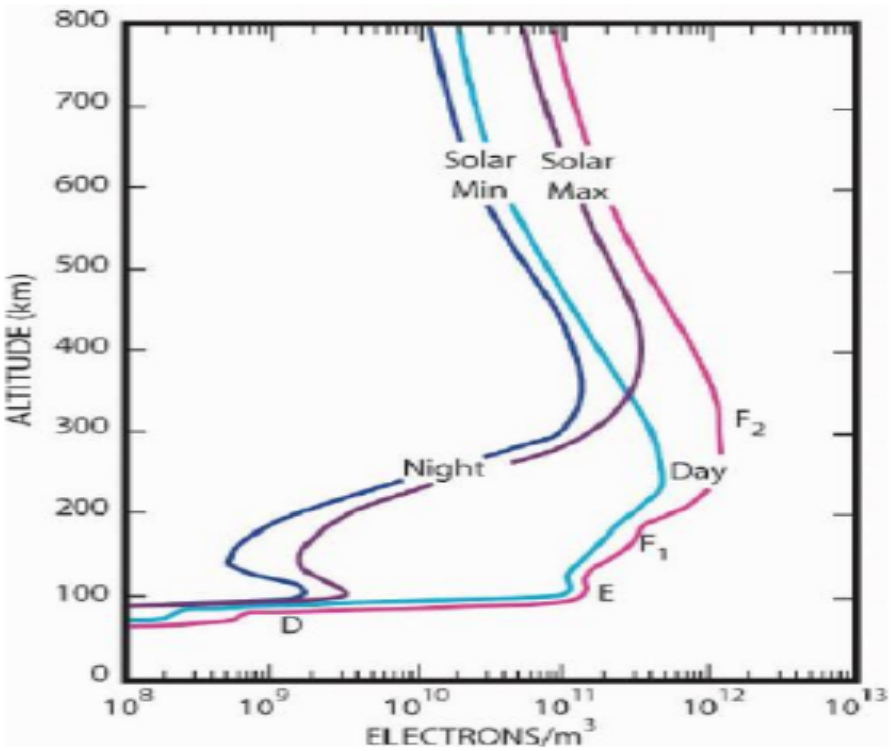

Figure 3.2: Typical ionospheric electron density profile.

The D-layer

It ranges from about 50 km to 90 km altitude above the Earth. In this layer, the primary source of ionization is cosmic radiation which is the same by day and by night manifesting itself in a strong solar cycle variation in the D−layer electron density. Despite this, by night, the electrons may become attached to atoms and molecules forming negative ions that cause the D−layer to disappear. By day, as a consequence of Sun's radiation, the electrons tend to detach themselves from the ions causing the D−layer electrons to re-appear. This region is the weakest region in terms of electron density distribution. The maximum electron density at noon reaches 1.5×10^4 cm^{-3}. Due to high rate of recombination rates in this region and low net ionization,

high frequency radio waves are not reflected by this layer. The D region is mainly responsible for high frequency (HF) absorption around 10 MHz and the absorption is higher at day time than night time. This layer greatly diminishes after sunset, but remains due to galactic cosmic rays [30].

The E−layer

The E−layer ranges from 90 km up to 140 km and the peak value of the electron density at day time is about $1.5 \times 10^5\ cm^{-3}$ and less than $10^4\ cm^{-3}$ during night time. The behavior of the E−layer almost entirely depends on the level of solar activity and the zenith angle of the Sun. The E−layer is free of disturbances unlike the D and F−layers and is only present by day. The primary source of ionization is the Sun's X−ray emissions resulting in electron densities showing distinct solar−cycle, seasonal and daily variations. The E−layer does not completely vanish at night, however, for practical purposes it is often assumed that its electron density drops to zero at night. The E region is dominated mainly by ionized molecular oxygen (O_2^+) and NO^+. Sometimes sporadic E is observed during day time but sporadic E is not common to see in the night time [10, 30].

The F−layer

The F region is the uppermost of the ionospheric regions and stretches from 140 km upwards, although current convention is to use the term ionosphere to refer to the region up to 1000 km altitude and the term plasmasphere to refer to the region of ionization above 1000 km. The F1 and F2−layers are the sub−component layers of the F−layer.

The F1−layer

The F1−layer is a daytime phenomenon and forms in the altitude range 140 to 210 km. The free electron density is about 10 times that of the normal E−region. Most radio waves propagating at oblique incidence that can penetrate the E region can also penetrate the F1−layer, so it has little effect on radio communications. The F1−layer peaks at 210 km with noon peak electron density of $2.5 \times 10^5\ cm^{-3}$, and disappears at night when combining with F2−layer to form the night time F−layer. The main source of ionization in the F1−layer is the EUV light. The F1−layer is only observed during the day since the electron densities are primarily controlled by the zenith angle of the sun. When it is present, it changes rapidly in a matter of minutes. It is more pronounced during the summer than during the winter months for low solar sunspot numbers and for periods with ionospheric storms.

The F2−layer

The F2−layer is the most important ionospheric layer from the point of view of HF propagation. The F2−layer is the highest layer in the ionosphere and also, normally, has the highest free electron density. This enhanced free electron density in spite of the fact that the extremely low density of the atmosphere at these heights means that the recombination rate is reduced significantly. However, even though the rate of ionization production is very low in the F−region and is decreasing with height, the loss due to recombination decreases even faster with height. The end result is that the electron density increases with height until diffusion becomes dominant, causing the electron density to then decrease with height, and hence the F2−peak is formed at about 300 km with peak electron density values of $10^6\ cm^{-3}$ at noon and $10^5\ cm^{-3}$ at

night times. The F2−layer's height and electron density is highly variable and large daily, seasonal and sunspot cycle variations are combined with the general behavior. Ionization is due to extreme ultraviolet radiation (EUV) ($10-100$ nm) solar radiation of atomic oxygen (O) [10, 30].

The topside region and the protonosphere

The topside ionosphere is the region above the F2−peak extended from about $600-1000$ km where the atomic Oxygen is dominant. In this region transport processes are the principal processes but production and loss are insignificant because the decrease in intensity of neutral particles increases diffusion processes. The electron density decreases exponentially with altitude in this region. Above the topside region, the region where lighter ions (H^+ and He^+) dominate is called the plasmasphere or protonosphere. This region is fully ionized region.

Ionization and Recombination

Ionization is the process in which electrons, which are negatively charged, are removed from (or attached to) neutral atoms or molecules to form positively (or negatively) charged ions and free electrons. An influx of electromagnetic radiation provides the energies needed to separate valence electrons from their atom or molecule. The solar emissions directed towards the Earth's atmosphere play the main role in the ionization process. The Sun's UV, emission ionizes the gaseous O, O_2, and N_2 molecules and produces free electrons and ionized particles. Solar radiation is responsible for the ionization process results in maximum free electron content of the ionosphere at 14 local time, just after local noon. The ionospheric electron density increases dramatically on the day side due to the increase of the UV, X-ray and photons [10].

After ions and electrons are produced in the ionization process, they will take part in chemical reactions in which they may disappear or produce other types of ions. At night particle energy levels drop to a level where more collisions occur, allowing recombination, producing neutral atoms. Atomic ions have much lower recombination than the molecular ions. Then in the F−region there are atomic ions and recombination is much smaller than the E and D−regions that contain molecular ions [27].

3.3 Variabilities of the ionosphere

3.3.1 Diurnal variation

The day and night electron density of the ionosphere is not the same. Night time electron densities are much lower than day time electron density because in night time the recombination rates are higher in the absence of ionization sources. The day time electron density reaches its peak value at noon hours. The ionosphere exhibits a diurnal variation where ionization is normally higher during the day and lower at night. As the Earth rotates with respect to the Sun, the intensity of the solar radiation increases and the ionization also increases to a maximum at around noon. Through the night, maximum frequencies gradually decrease, reaching their minimum just before dawn [31].

3.3.2 Seasonal variation

The ionosphere exhibits strong seasonal and solar-cycle variations because the main source of ionization and energy for the ionosphere is photo-ionization. Therefore, whenever there is a change in solar zenith angle or the solar radiation fluxes, the

ionosphere will change. As the Earth revolves around the Sun, a seasonal cycle is generated, determined by which hemisphere the Sun is overhead. It is summer on the hemisphere where the Sun is overhead and winter on the other hemisphere.

The Sun is overhead at the equator around the time of the equinoxes. This seasonal cycle causes a corresponding seasonal and spatial variation in the global ionospheric structure. The D, E and F1−region electron densities are greater in summer than in winter. However, the variation in F2−region electron densities is more complicated. In both hemispheres, electron densities generally peak around the equinoxes [31]. Around solar minimum the summer noon electron densities are, as expected, generally greater than those in winter, but around solar maximum winter frequencies tend to be higher than those in summer a phenomenon called seasonal anomaly. In addition, frequencies around the equinoxes (March and September) are higher than those in summer or winter for both solar maximum and minimum [32].

3.3.3 Solar cycle variation

Measurements of the sunspot number, an indicator of solar activity, show that the Sun goes through a periodic rise and fall in activity with a period of about 11−years. Since ionization is driven by solar electromagnetic and corpuscular radiation, it is a function of solar activity. At solar maximum the Sun emits more radiation and therefore ionization is greater. Thus the critical frequencies of the ionospheric layers are greater during high solar activity periods [10].

3.3.4 Latitudinal variations

The diurnal and seasonal behaviors observed the Sun's position relative to the atmosphere plays significant role in latitudinal variation in the ionospheric electron density

because the solar zenith angle (χ) measured from the observer's local vertical to the Sun determines the intensity of ionization. This shows that as the solar zenith angle becomes smaller the ionosphere exposes to higher radiation rates and ionization becomes larger. Ionization is produced almost entirely by UV and X-ray emissions from the Sun, and is depleted again by chemical recombination [33].

3.4 Ionospheric disturbances

Ionospheric disturbances can result from solar disturbances or geomagnetic field disturbances. The ionospheric disturbances are associated directly or indirectly with the events on the Sun. The geomagnetic disturbances are also caused by events initiated from the Sun, however, these events rather affect the outermost geomagnetic field line (also called the magnetopause) and compress the geomagnetic field causing the geomagnetic disturbances.

3.4.1 Ionospheric storms

Solar activity such as flares and coronal mass ejections often produce large variations in the particle and electromagnetic radiation incident upon the Earth. Such variations can, in turn, lead to disturbances of the quiet-time magnetosphere and ionosphere. These disturbances, when affecting the ionosphere are known as ionospheric storms, tend to generate large disturbances in ionospheric density distribution, total electron content, and the ionospheric current system. Ionospheric storms have important terrestrial consequences such as disrupting satellite communications and interrupting the flow of electrical energy over power grids [28].

3.4.2 Geomagnetic storms

A geomagnetic storm is a worldwide disturbance of the Earth's magnetic field, associated with solar activity when there is a very efficient exchange of energy from the solar wind into the space environment surrounding Earth. These storms result from variations in the solar wind that produces major changes in the currents, plasmas, and fields in Earth's magnetosphere. The solar wind conditions that are effective for creating geomagnetic storms are sustained (for several seconds to many hours) periods of high-speed solar wind, and most importantly, a southward directed solar wind magnetic field (opposite the direction of Earth's field) at the dayside of the magnetosphere. This condition is effective for transferring energy from the solar wind into Earth's magnetosphere.

The largest storms that result from these conditions are associated with solar coronal mass ejections (CMEs) where a billion tons of plasma from the sun, with its embedded magnetic field, arrives at Earth. CMEs typically take several days to arrive at Earth, but have been observed, for some of the most intense storms, to arrive in as short as 18 hours. Another solar wind disturbance that creates conditions favorable to geomagnetic storms is a high-speed solar wind stream (HSS). HSSs plow into the slower solar wind in front and create co-rotating interaction regions, or CIRs. These regions are often related to geomagnetic storms that while less intense than CME storms, often can deposit more energy in Earth's magnetosphere over a longer interval [4].

Geomagnetic storms, in which the global geomagnetic field intensity decreases

on the order of tens to hundreds nT, are large scale phenomena in the solar wind-magnetosphere-ionosphere coupling. Geomagnetic storms develop when solar wind-magnetosphere couplings are intensified by solar wind disturbances coming out through coronal holes and coronal mass ejections (CMEs). Basically there are two major types of storms: CME driven geomagnetic storms and CIR driven Geomagnetic storms. The geomagnetic storms driven by both are not the same. The characteristics of the storms driven by both CME and CIR are not the same type. The storm driven by the fast CMEs are usually very intense with $Dst < -100$ nT, while the storm driven by CIRs are usually weaker and their main phase has irregular profile and long recovery phase lasting many days to weeks and cause high intensity long duration continuous activity as shown in Fig. 3.3. CIRs arrive at Earth with physical properties somewhat similar to those of the interplanetary CMEs (ICMEs). Although the profiles of these two different magnetic storms are qualitatively similar, the physical causes and characteristics of the different storm phases are different. Magnetic storm starts with sudden increase of the intensity of the geomagnetic field horizontal component, called Storm Sudden Commencement (SSC). The southward interplanetary magnetic field reconnection in the day side magnetosphere, rapidly injecting magnetic field and particle energy into the Earth's magnetosphere and modifying the large scale ring current system. As a result of reconnection, it leads to aurora formation, geomagnetic storm phenomena, and enhanced ring current system [5, 6].

Ring current

Electrically charged particles trapped in Earth's magnetic field experience an equatorial drift motion resulting in westward flowing ring current in the equatorial plane. The ring current is one of the major current systems in the earth's magnetosphere.

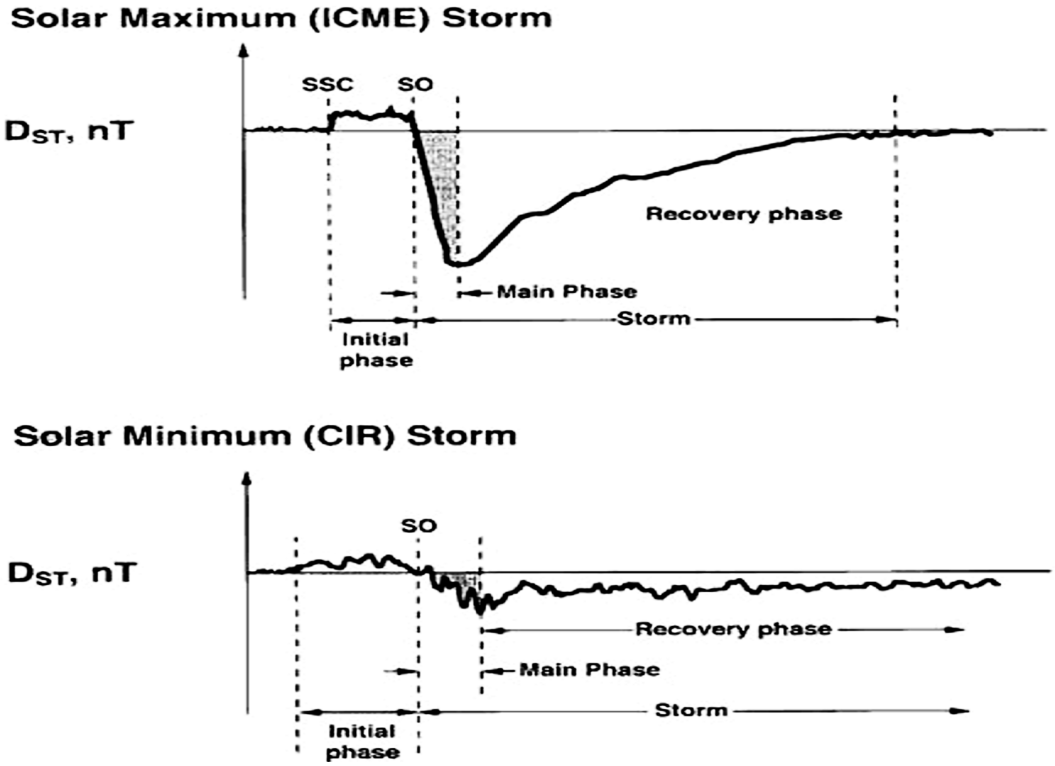

Figure 3.3: Schematic of a magnetic storm generated by an ICME (top) and by a CIR (bottom). Taken from Tsurutani (2000).

It circles the Earth in the equatorial plane and is generated by the longitudinal drift of energetic (10 to 200 keV) charged particles trapped on field lines between $L \sim 2$ and 7. Basically the interconnection between southward interplanetary magnetic field and Earth's magnetic field leads to strong dawn-to-dusk electric fields and this overall increase in magnetosphere convection and causes intense ring current buildup and storms [34]. During geomagnetic storms, ring current particle fluxes are dramatically increased, with the peak enhancements occurring in the inner ring current (at $L < 4$). The quiet-time ring current consists predominantly of H^+, while the storm-time ring current also contains a significant component of ionospheric O^+, whose contribution to ring current energy density may even exceed that of H^+ for brief periods near

the maximum of particularly intense storms. The formation of the storm-time ring current has been attributed to two different processes: (i) the injection of plasma into the inner magnetosphere during the expansion phase of magnetospheric substorms and (ii) increased convective transport of charged particles from the nightside plasma sheet deep ($L < 4$) into the inner magnetosphere as a result of an intensification of the earth's dawn-dusk convection electric field during extended periods of strong southward IMF. The present understanding of ring current formation tends to favor the enhanced convection model over the substorm plasma injection model; however, it is recognized that substorms, while not the primary driver, nonetheless play a significant role in the growth of the storm-time ring current (e. g., by energizing ions in the near-earth plasma sheet prior to their transport into the ring current). The storm-time growth of the ring current lasts from 3 to 12 hours and constitutes the main phase of a magnetic storm. Following this main phase, the ring current begins to decay, returning to its pre-storm state in two to three days. Full recovery can require as long as a month in the case of major geomagnetic storms. During the storm recovery phase, particle transport into the ring current slows, allowing various loss processes to reduce ring current particle fluxes to their quiet-time level. The primary loss process during both the main and recovery phases is charge exchange with neutral hydrogen atoms in the geocorona. The storm level of geomagnetic storms can be characterized using different geomagnetic indices.

3.4.3 Magnetic indices

In the absence of direct measures of activity in the ionosphere and magnetosphere, the geomagnetic indices are used as proxies for the solar and geomagnetic disturbance levels. These magnetic indices were primarily intended to define discrepancies in the

geomagnetic field, triggered by irregular current systems between the magnetosphere and ionosphere. Commonly these indices are derived from parameters which are monitored continuously with ground-based equipment. The Space Weather Scientific Community mostly makes use of the Kp, Ap and Dst indices [5, 6], in which the Dst index is briefly described as follows while the rests are described in accordance with our results and discussion parts.

Disturbance storm time index

The Dst is a geomagnetic index which monitors the world wide magnetic storm level. It is constructed by averaging the horizontal component of the geomagnetic field from mid-latitude and equatorial magnetograms from all over the world. Negative Dst values indicate a magnetic storm is in progress, the more negative Dst is the more intense the magnetic storm. The negative deflections in the Dst index are caused by the storm time ring current which flows around the Earth from east to west in the equatorial plane. The ring current results from the differential gradient and curvature drifts of electrons and protons in the near Earth region and its strength is coupled to the solar wind conditions. Only when there is an eastward electric field in the solar wind which corresponds to a southward interplanetary magnetic field (IMF) is there any significant ring current injection resulting in a negative change to the Dst index. Thus, by knowing the solar wind conditions and the form of the coupling function between solar wind and ring current, an estimate of the Dst index can be made [35, 36].

3.5 Ionosphere Probing Techniques

3.6 Global Navigation satellite System (GNSS)

The Global Positioning System (GPS) is a constellation of navigation satellites operated by US Department of Defence (DOD) [1]. GPS became operational since 1980 and consists of at least 24 operational satellites distributed in 6 orbital planes with 4 satellites per plane. The satellites are placed at an altitude of $20,200$ Km above the Earth with 12 hrs orbital period and 55^0 orbital inclinations. The time, velocity and position of GPS satellites are continuously monitored by ground based networked radars and up to 12 satellites are visible at a time. GPS satellites transmit their individual ephemeris on two carrier frequencies in the L-band for civilian users $f_1 = 1575.42$ MHz (L_1) and $f_2 = 1227.60$ MHz (L_2). Each GPS signal consists of three components namely carrier, code and navigation data. These three components of the signal are derived coherently from one of the atomic standards aboard the satellite. The frequency of the atomic standards aboard a satellite is 10.23 MHz. GPS signals, like other electromagnetic waves, are affected by the electrically charged ionised plasma in the upper atmosphere [26, 31, 37].

Global navigation satellite system (GLONASS) is the Russian navigation system equivalent to GPS. Again its constellation is composed of 24 satellites with an orbital inclination of 64.8^0 and an orbital radius of $25,500$ km. Also GLONASS satellites transmit signals on the L_1 and L_2 frequency bands, each satellite transmits its signal with different frequency offset. So to distinguish from GPS carriers G_1 and G_2 are used. Like the GPS, GLONASS is also a dual$-$use, i.e for civilian and military purposes.

Galileo is the European global navigation satellite system. Unlike the GPS and GLONASS, Galileo is under civilian control. The Galileo satellite constellation will consist of 30 satellites (27 operational and 3 non-functional). The satellites are orbiting at an altitude of $29,600$ Km at inclination of 56^0.

Compass is a Chinese satellite navigation system which is presently under development. The system is a dual system which will provide two navigation services (an open services for commercial users and for an Authorizesd persons). Compass consists of constellation of 30 non$-$stationary satellites, 5 geostationary satellites and 3 more satellites in geosynchronous orbit. The first non$-$stationary satellites are in three orbital planes with an inclination of 55^0 at an orbital radius of $27,900$ km. While the geosynchronous once are at an altitude of 3585 km and inclination 55^0 [26, 31, 38].

3.6.1 Ionospheric effects on electromagnetic waves

The ionosphere is a dispersive medium, thus a linear combination of observable on the two frequencies is needed to remove this effect for positioning. On the other hand the dispersive property provides an opportunity to measure directly the ionospheric electron content along the ray path. The travel time of an electromagnetic wave through a medium with refractive index n is given as

$$t_{travel} = \int_{raypath} \frac{1}{c_{medium}} dr \tag{3.1}$$

The phase refractive index as a function of the frequency is

$$n^2 = 1 - \frac{\omega_p^2}{\omega^2} \tag{3.2}$$

where $\omega_p^2 = \frac{Ne^2}{\varepsilon_0 m_e}$ is the plasma frequency

Solving Eq. (3.2) for small n and Taylor expansion, we have

$$n = 1 - \frac{\omega_p^2}{2\omega^2} = 1 - \frac{Ne^2}{8\pi^2\varepsilon_0 m_e f^2} \tag{3.3}$$

and using $A = \frac{e^2}{8\pi\varepsilon_0 m_e} = 40.3\frac{m^3}{s^2}$ we can write

$$t_{travel} = \frac{1}{c}\int_{raypath} 1 - \frac{AN(\vec{r})}{f^2} d\vec{r} \tag{3.4}$$

The ionospheric phase delay relative to wave propagation in a vacuum is

$$I_{phase} = t_{travel}^{medium} - t_{travel}^{vacuum} = -\frac{A}{cf^2}\int_{raypath} N(\vec{r}) d\vec{r} \tag{3.5}$$

The minus sign in Eq. (3.5) indicates the phase is advanced so Eq. (3.3) has the form

$$n_g = 1 + \frac{\omega_p^2}{2\omega^2} \tag{3.6}$$

Therefore the average group is delayed by

$$I_{group} = t_{travel}^{medium} - t_{travel}^{vacuum} = \frac{A}{cf^2}\int_{raypath} N(\vec{r}) d\vec{r} \tag{3.7}$$

Thus the group delay is equal to the negative of the phase advance [39]. The phase of the GPS carrier wave is advanced by the same amount of time that the information in a wave group is delayed. The latter integral in Eq. (3.5) and (3.7) is simply the electron density integrated along the ray path from satellite to receiver, which is called the Total Electron Content (TEC). Therefore TEC can be calculated as [40]:

$$TEC = \int_{raypath} N(\vec{r}) d\vec{r} \tag{3.8}$$

The total electron content along the GPS ray path from a satellite to a receiver is known as slant TEC (STEC). TEC is the number of electrons in the slant column with unit squared cross−section in the ionosphere along the signal path. It is expressed in

TECU (TEC−Units) with $1TECU = 10^{16}$ electrons.m^{-2}. The STEC can be obtained from the difference between the pseudo ranges (P_1 and P_2), and the difference between the phases (L_1 and L_2) of the two GPS signals ([41] and references therein). The relevant equations are

$$STEC_{co} = [(\frac{f_2^2}{f_1^2 - f_2^2})\frac{2f_1^2}{K}](P_2 - P_1) \tag{3.9}$$

$$STEC_{ph} = [(\frac{f_2^2}{f_1^2 - f_2^2})\frac{2f_1^2}{K}](L_1\lambda_1 - L_2\lambda_2) \tag{3.10}$$

where f_1 and f_2 are GPS signal frequencies and are equal to 1.57542 GHz and 1.2276 GHz, respectively, $K = 80.62\ m^3s^{-2}$ is a constant that relates plasma frequency to electron density, λ_1 and λ_2 are the wavelengths corresponding to f_1 and f_2.

3.6.2 Single layer ionosphere approximation

The TEC is valid for line of sight from the receiver on the ground to the satellite. The ionosphere may be considered as a thin single layer surrounding the Earth at a fixed height from the Earth for which all the free electrons in the ionosphere are assumed to be concentrated in a single layer thin shell at the height of the main electron concentration in the ionosphere. In addition to that if we assume there are no lateral or horizontal electron density gradients, the vertical TEC (VTEC) can be simply mapped to the slant TEC:

$$STEC = \frac{1}{\cos\zeta} VTEC \tag{3.11}$$

where ζ is the satellite zenith angle at the point of intersection of the line of sight with that of the spherical single layer ionosphere called the ionospheric piercing point (IPP) and the multiplier $\frac{1}{\cos\zeta}$ is called the obliquity factor. The vertical projection of

IP on the ground is referred as the sub-ionospheric point (SIP). The satellite zenith angle at the receiver location $\zeta^{'}$ and at the ionospheric pierce point is related by

$$\sin\zeta = \frac{R}{R+H}\sin\zeta^{'} \tag{3.12}$$

where H is height of the ionospheric single layer from the Earth and R is the radius of the Earth.

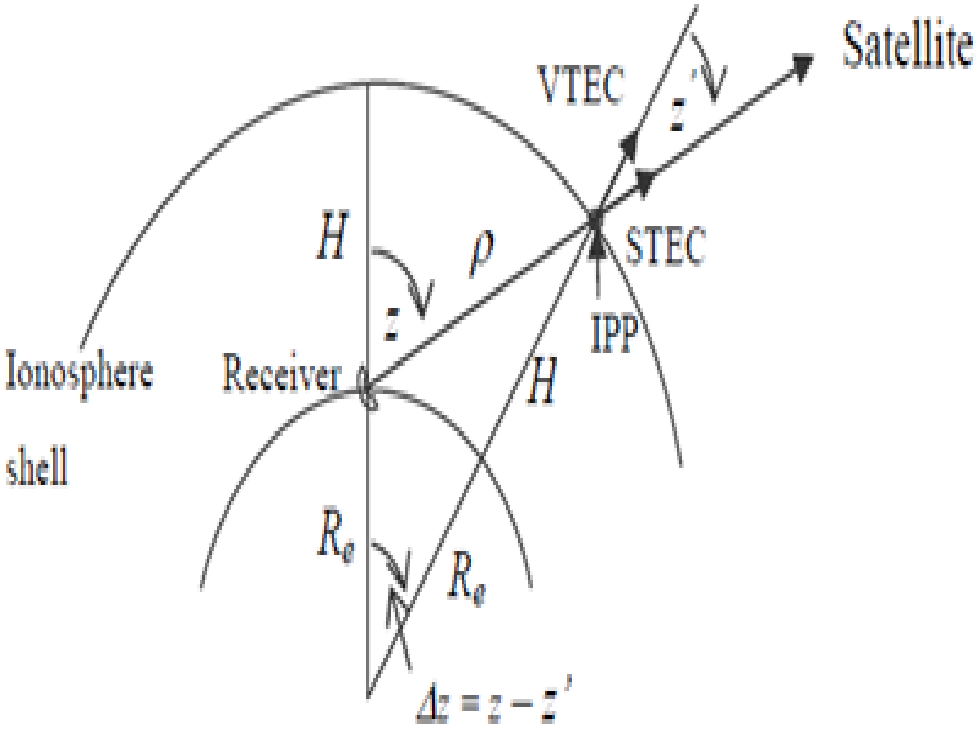

Figure 3.4: Slant to vertical TEC mapping function geometry.

3.7 Conventional ionospheric measurements: the ionosonde

The conventional instrument for measuring the virtual height of the ionosphere is a sweep-frequency pulsed radar device called the ionosonde. An ionospheric sounding consists of vertical sweep of the ionosphere by a predetermined frequency band (< 30 MHz)with a sweep duration from few seconds (e.g. 10 second) to few minutes. During reflection electron density values are calculated from reflected radio waves corresponding to the density dependent critical frequency (f_p) of the ionized plasma and density heights are inferred from the time delay of the reflected radio waves. The ionosonde provides estimates electron density maxima of each layer and the estimated altitude at which the density occurred, as a function of time. The ionosphere is a dispersive medium so the electromagnetic wave reflection depends on the signal frequency of the wave. In the presence of magnetic field of the Earth, the ionosphere is doubly reflecting medium, and two modes of propagation exist for which names, ordinary and extraordinary. Assuming collision of ions with neutrals is negligibly small, the refractive index from the Appleton and Hartree [42] is well explained and can be expressed as:

$$\mu^2 = 1 - \frac{X(1-X)}{(1-X) - \frac{1}{2}Y_T^2 \pm [\frac{1}{4}Y_T^4 + (1-X)^2 Y_L^2]^{\frac{1}{2}}} \tag{3.1}$$

where $X = \frac{\omega_p^2}{\omega^2}$, $Y = \frac{\omega_H}{\omega}$, $Y_T = Y \sin\theta$, and $Y_L = Y \cos\theta$ Assuming plasma is horizontally stratified, a wave vertically incident on the ionosphere is reflected at a level where $\mu^2 = 0$ and this occurs for ordinary wave, where $X = 1$. The relation between the electron density and the critical frequency is given by

$$N_e = \frac{4\pi^2 m f^2 \varepsilon_0}{e^2} \tag{3.2}$$

where N_e is the electron density (number of electrons per cubic meters); f is frequency of radio wave which $f = f_p$; e and m are charge and mass of electron respectively; ε_0 is permittivity of vacuum which is $8.85 \times 10^{-12}\ F.m^{-1}$.

The ionosonde consists of transmitter and receiver with coupled tuning circuits, which is a sweep in frequency usually in a frequency range of $0.5 - 25$ MHz. After the RF signals have been reflected by the ionosphere they are received and processed by the receiver to produce ionograms. The basic information in the received signal in the transit time for passage between the ionospheric layers and the Earth, frequency, amplitude, phase polarization, doppler shift and spectrum shape [42].

Limitations of all ionosondes is that they can give information on the ionosphere only up to the height of maximum ionization of the F2−layer, again unless one extends end of the sweep (to at least 250 KHz), by an increasing the height of the transmitting antenna tower and using relatively higher power not much information can be obtained from the D−region. Because low frequency radio waves are absorbed by the D−region. During sudden ionospheric disturbances (SIDs) and intense polar cap precipitation of solar energetic particles, D−region ionization can become so intense that HF radio communication is completely blacked out so information from ionosonde is limited.

Chapter 4

Data and Methodologies

4.1 Data

The observational datas used are described as follows. To study the Solar activity, diurnal and seasonal variations and space weather events of ionospheric TEC over Ethiopia, GPS data from January to December 2015 for all days at Addis Ababa and Bahir Dar stations using a dual frequency f_1(1575.42 MHz) and f_2(1227.60 MHz) have been downloaded from UNAVCO data home page:

$(http://facility.unavco.org/data/gnss/perm-sta.php)$.

The data for Dst index is downloaded from world data center web cite: $(wdc.kugi.kyoto-u.ac.jp/dst\_realtime/presentmonth/index.html)$. The Dst value for geomagnetically quite days prior to storm occurrence is greater than -20 nT whereas the Dst values during the storm period fall in moderate storm category. The observed changes of geomagnetic field during geomagnetic storm are essentially a consequence of strong and rapid magnetospheric processes and changes under solar wind action. The geomagnetic storms can be classified according to different Dst index levels as: weak for $-50 \leq Dst \leq -30$ nT; moderate for $-100 \leq Dst \leq -50$ nT and intense for $Dst < -100$ nT (e.g. [43, 44] and references therein).

The data on solar wind parameters such as plasma flow pressure/solar wind pressure (PSW), solar wind speed (Vsw), interplanetary electric field (IEF) Esw, the H-component of symmetric ring current ($SYM-H$), H-component of asymmetric ring current ($ASY-H$), the auroral electrojet (AE) indices and solar proton event (SPE) with energies of $E>10$ MeV, $E>30$ MeV and $E>60$ MeV are downloaded from the database available with coordinated data analysis web page: ($http://cdaweb.gsfc.nasa.gov/istppublic/$). It contains the values of the interplanetary magnetic field (IMF) and solar wind parameters measured by various spacecrafts (ISEE3, IMP8, etc.) near the Earth's orbit.

4.2 Data analysis methodologies

After all the datas are received from the source, MATLAB programming with its code has been developed by importing the data. Using the MATLAB programming code the value of TEC in Addis Ababa and Bahir Dar stations for all days of each month and season including selected disturbed and undisturbed days has been plotted as shown in the results stated in chapter 5. Similarly, SSN, Radio flux and Dst index of selected months of 2015 and data on solar wind parameters such as plasma flow pressure/solar wind pressure (PSW), solar wind speed (Vsw), interplanetary electric field (IEF)Esw, the H$-$component of symmetric ring current ($SYM-H$), H$-$component of asymmetric ring current ($ASY-H$) and the auroral electrojet (AE) indices are also plotted using the obtained loaded data from the web sites by importing in to MATLAB and creating programming code to show the solar activity and geomagnetic storm conditions of the Earth's ionosphere.

Chapter 5

Results and Discussions

5.1 Introduction

The results presented here are from the analysis of TEC values measured by two independent GPS receivers situated at a distance of around 500 km apart and very close to the geographic equator in Ethiopia, East Africa. By analyzing TEC data at the two stations during the year 2015, we demonstrated the diurnal, monthly and seasonal variations of TEC, its dependence and Variation with solar activity and Space Weather Events by using solar activity (sunspot and radio flux) and geomagnetic activity (solar wind) indices.

5.2 Diurnal variation of Ionospheric TEC

The diurnal variation of the electron density can be studied using TEC parameter. Fig. 5.1 shows the diurnal variation of the TEC in the year 2015 around peak of solar cycle 24. TEC value has its maximum at noon time and is very low during night time. The plots show TEC (TECU) versus universal time (UT) in hr in the year 2015 at an elevation mask angle 30^0 at Addis Ababa and Bahir Dar stations, in Ethiopia. The

TEC variation is not only time dependent it also depends on latitude. The variations with low at night time TEC value and peaks at noontime is the typical behavior of the ionosphere. As the sun is the main source of ionization most TEC variations are resulted due to the activity of the Sun. However, the modifications of the atmosphere from below can not be neglected [45, 46].

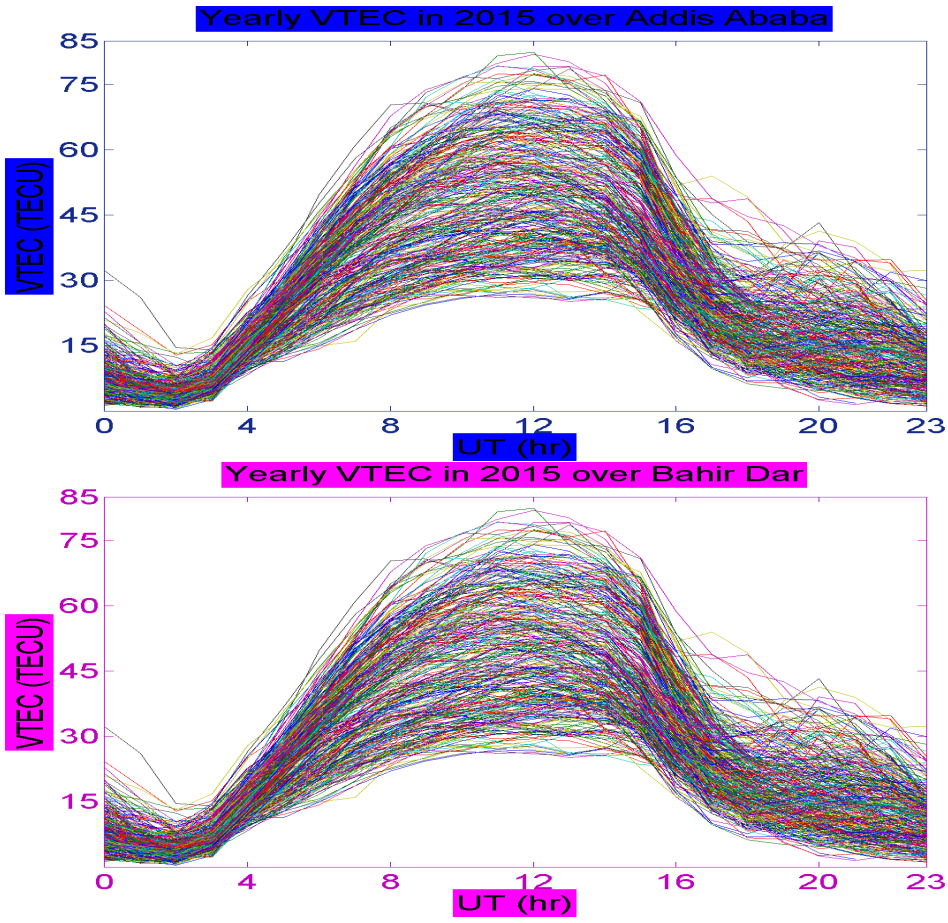

Figure 5.1: Mass plot of VTEC at Addis Ababa and Bahir Dar stations during 2015.

The diurnal patterns of TEC exhibits a steady increase starting about sunrise to an afternoon maximum and falls to attain a minimum just before sunrise. The diurnal characteristic of TEC has seasonal, solar activity, geomagnetic activity and

latitudinal dependence. As clearly indicated in Fig. 5.2, the magnitude of GPS TEC

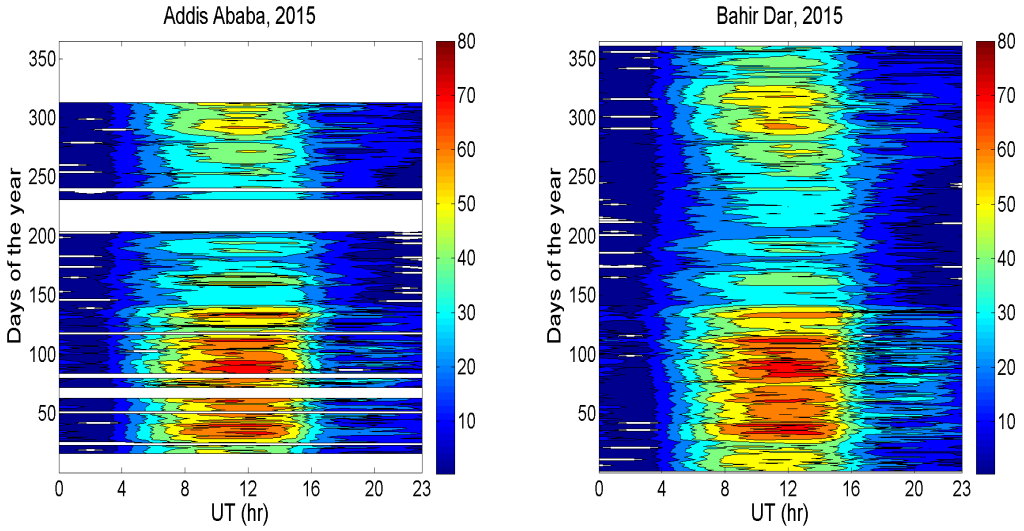

Figure 5.2: Contour plots of the diurnal variation in GPS-TEC measured at the study areas in Ethiopia. The white sections in the plots show unavailability of the data.

is generally high during day time at both locations. The day time GPS-TEC values are generally greater than the night time values. This can be attributed to the absence of solar radiation at night time. After this general observation we are interested to observe the overall and indepth phenomenas happened in each months of days during the selected year for this study.

As observed from Fig. 5.2 due to the incompleteness of the data at Addis Ababa station during certain days of months, we presented the diurnal variations by using Bahir Dar station dual frequency GPS-TEC data. The diurnal variation in TEC at Bahir Dar, Ethiopia exhibits many characteristics typical to low (equatorial) latitude ionosphere such as a TEC minimum at predawn and gradual increase with the time of day attaining a maximum in the afternoon and a gradual decrease after sunset.

The daily peak occurs at about $0900 - 1500$ UT (around 1200 UT) around low latitude (equatorial) regions. In equatorial regions or low latitude the daily variation peak TEC greatly depends on Sun's activity. The day to day variability of TEC is contributed by the various parameters like EUV, solar flares and CME [47].

Figs. 5.3 to 5.8 shows the mass plot of TEC diurnal variation for the different days of the year 2015. In all these plots the diurnal variations show a maximum occurring around $0900 - 1500$ UT and short-lived minimum in TEC occurring around $0000 - 0800$ UT and $1600 - 2300$ UT. Generally this temporal variation is depending on intensity of radiation coming from the Sun, since the intensity increases starting from sunrise and becoming maximum when Sun is overhead and comes to zero when sunset.

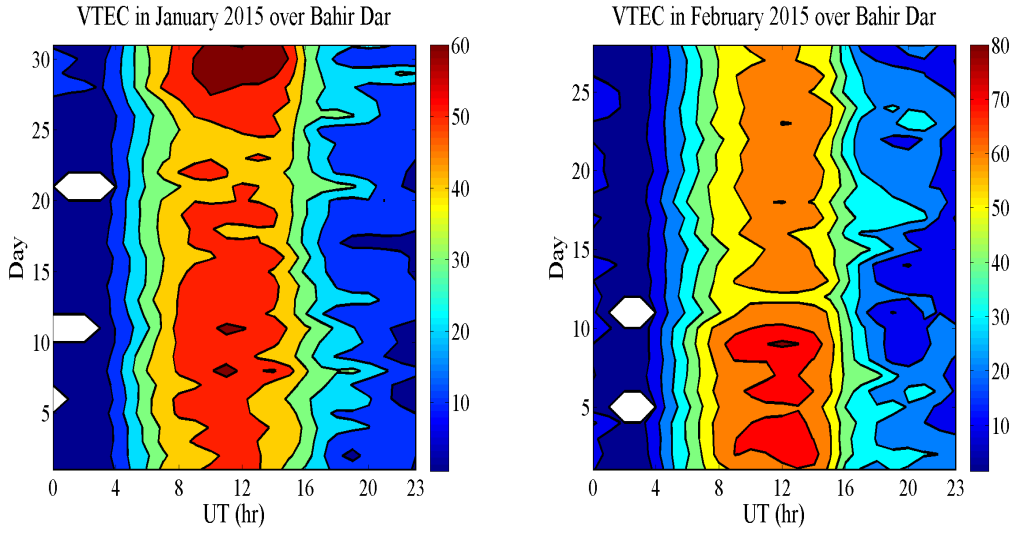

Figure 5.3: Diurnal variation of TEC observed at Bahir Dar station during January and February, 2015.

As observed from Fig. 5.3, concentration of TEC is greater between $0900 - 1500$ UT, maximum TEC is observed during January 30 and during February $1 - 10$, 13,

19 – 25 and 28, 2015. Around January 4, 2015 it seems the least TEC measured. From Fig. 5.4, we observe that the concentration of TEC value observed in March is

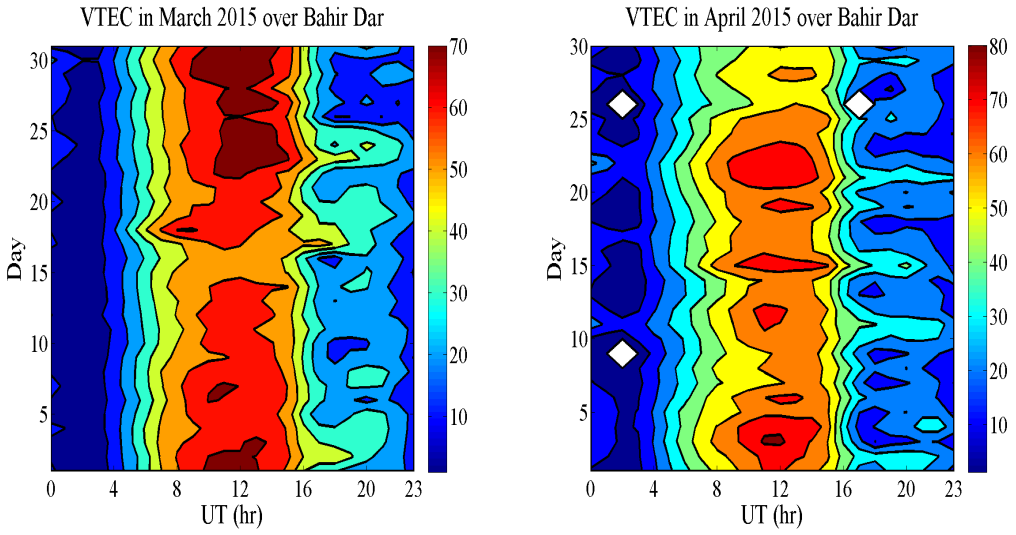

Figure 5.4: Diurnal variation of TEC observed at Bahir Dar station during March and April, 2015.

maximum between 0900 – 1500 UT. The peak TEC measured on March 30 afternoon at 1100 UT. In the morning and evening the amount of TEC is similar and less than the peak value. On the other hand maximum TEC around 80 TECU measured in April.

In Fig. 5.5, Peak TEC of 68 TECU were observed in may 11 – 15, 2015. However, in June 5, 2015 exhibited TEC maximum peak value is about 39 TECU while on June 23, 42 TECU were recorded. On June 23, there is a geomagnetic storm occurred on Earth's magnetosphere and we observe the phenomena in depth on the last section of this chapter. From Fig. 5.4 and Fig. 5.6, the least peak TEC observed from the station during the days in the two months namely July and August. On July 5 – 8 and 11 – 14 and August 27 – 30, 2015 peak TEC were measured later after noon at

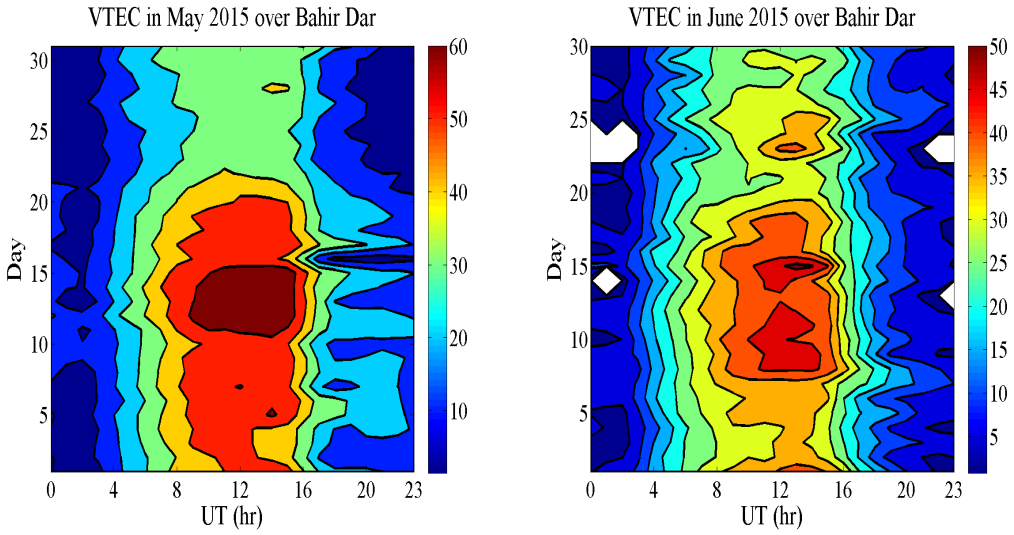

Figure 5.5: Diurnal variation of TEC observed at Bahir Dar station during May and June, 2015.

$0800 - 1500$ UT.

Based on Fig. 5.7 we can generalize that, the derived GPS ionospheric TEC value is maximum during late days of September and October as compared to June, July and August. In September 29 peak measured TEC were about 56 TECU, while on October 18, 64 TECU peak value were measured. From Fig. 5.8, we observe that during November similar peak TEC of magnitude 63 TECU were measured. From $2 - 3$ and $11 - 16$, December, 2015 at $0800 - 1500$ UT the derived TEC value was maximum. From the indicated days some how the solar activity was maximum then the GPS station drives strong TEC value. December month is an element of winter season, we expect the TEC value is intermediate so does the obtained result.

In all above Figs. $(5.3 - 5.8)$ the TEC value of one day is different from the TEC value of another day of the same month. These day to day variations of TEC may be attribute to the change in activity of the Sun itself. This means that, sunspot number,

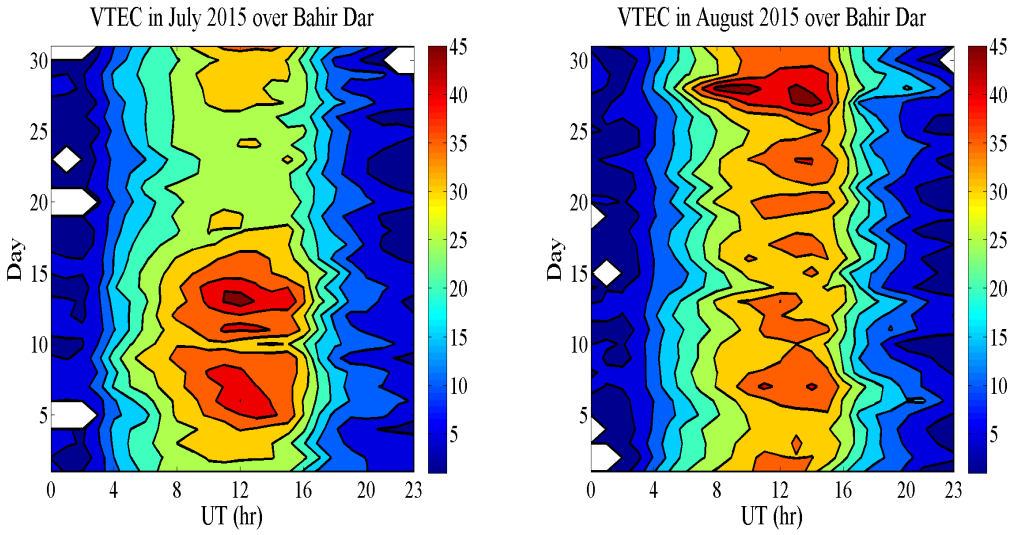

Figure 5.6: Diurnal variation of TEC observed at Bahir Dar station during July and August, 2015.

geomagnetic activity and different particles coming from the Sun are different from day to day so that the TEC value varies accordingly. Moreover, the maximum VTEC is obtained at the day time near noon. As it is known, the intensity of the sun's radiation is influenced by the angle of the Sun's rays striking the atmosphere. At noon time the intensity of light from the Sun is relatively large compared to the other hours of the day. Thus, photo-ionization processes are maximum and maximum TEC is obtained at noon time. During the night time the value of TEC is very small because electrons lost as a result of the recombination processes.

In general, Fig. 5.3 to Fig. 5.8 shows the diurnal and hourly variation of TEC at Bahir Dar station in the year of 2015. In all these contour plots the diurnal variations show a maximum occurring of TEC is found between $0900-1500$ UT and short-lived minimum in TEC occurring around $0000-0800$ UT and $1600-2300$ UT. The trend of this result is in accordance with the diurnal variations in TEC at Adama station

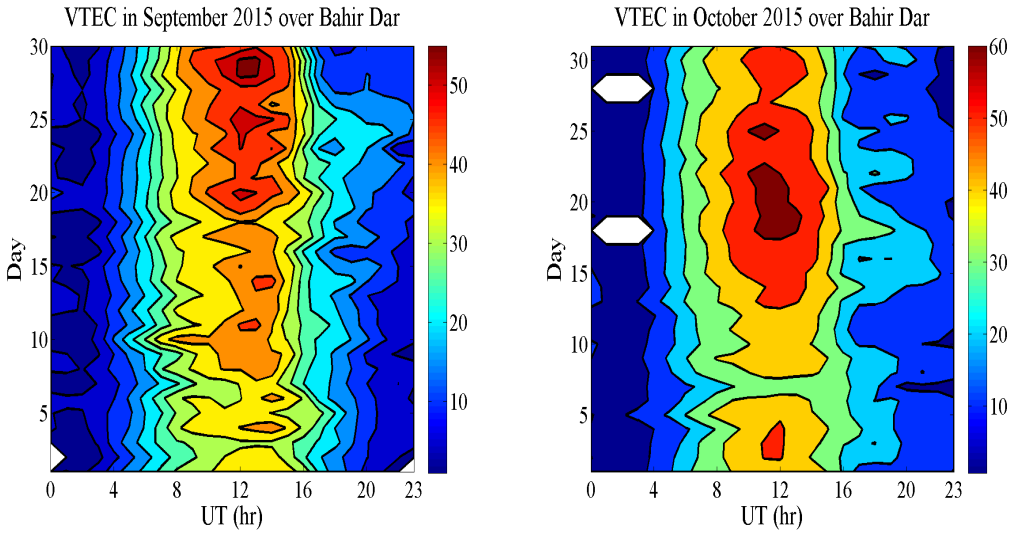

Figure 5.7: Diurnal variation of TEC observed at Bahir Dar station during September and October, 2015.

in the works of Amensisa et al. [48], and others showed that the diurnal variation in TEC shows a short lived predawn minimum, a steady early morning increase, followed by an afternoon maximum and gradual fall after sunset.

5.3 Monthly Variation of Ionospheric TEC

Fig. 5.9 shows that there are significant VTEC differences in both magnitude and pattern over 12 months period in the two stations in the build up region, afternoon plateau and decay region. In all months the TEC value is maximum near noon and of all months the highest TEC is obtained around noon. In Addis Ababa station, the month of March recorded the highest peak TEC of 68.4 TECU at about 1100 UT followed by February and April with Peak TEC of 66.16 and 64.5 TECU at about 1200 and 1100 UT respectively. The least peak TEC of 37.4 TECU and 36.67 TECU at about 1200 UT and 1300 UT was observed in July and August respectively. In

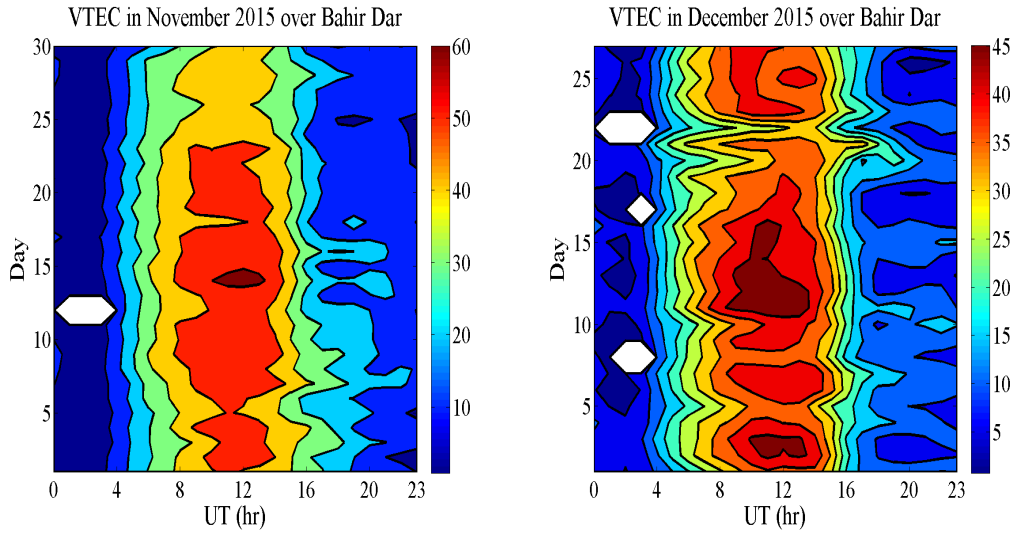

Figure 5.8: Diurnal variation of TEC observed at Bahir Dar station during November and December, 2015.

Bahir Dar station, the month of March recorded the highest peak TEC of 69 TECU at about 1200 UT followed by April and February with maximum TEC value of 68 TECU and 67 TECU at about 1100 UT respectively, during the year 2015. The month of July recorded the least peak TEC of 32 TECU at about 1100 UT.

The variation of the monthly median TEC for the above mentioned period of 12 months for the two stations are as shown in the contour plots of Fig. 5.9. The features mentioned above are reflected very well in this Figure. The minimum median TEC was registered from $1600 - 0700$ UT except in the months of March, April and February where the periods of $1600 - 0700$ UT recorded moderate median TEC values during these months. The afternoon maximum was attained between the hours of 0900 and 1500 UT. The months of June, July and August recorded moderate median TEC values ranging from 36 to 38 TECU during the afternoon maximum. The highest median TEC values was recorded in the months of January, March, April,

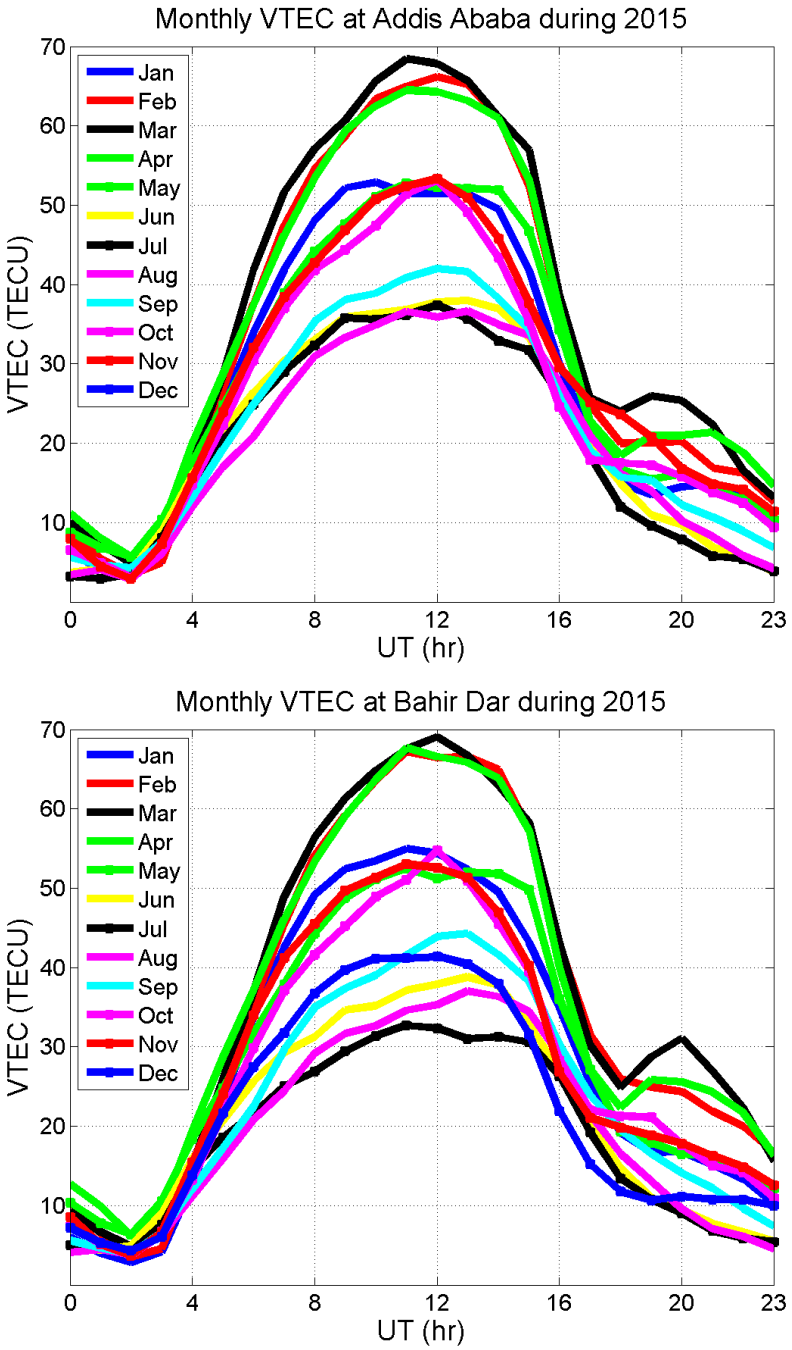

Figure 5.9: The median monthly Variation of TEC observed at Addis Ababa and Bahir Dar Stations during 2015.

February and October with values ranging from $64-69$ TECU. The exceptional peak value of the derived TEC for March, 2015 were because of it is an element of the equinoctial season, as we know, in this season the magnitude of TEC is maximum near the equator (low latitude region) due to the Zenith angle of the Sun is towards to the equator (e.g Addis Ababa and Bahir Dar ionospheric sectors are near to low latitude region). In more general case the peak TEC values reach first in Addis Ababa as compared to Bahir Dar.

Our ionospheric sector has been produced too much amount of free electrons during the day time. One can deduce from Fig. 5.9 there is strong TEC recorded throughout the whole months in the time about $0900-1500$ UT. During February, March and April 2015 the magnitude of the TEC is better than the rest days of other months at $0000-2300$ UT. The three months (March, April and February) TEC value during 2015 at both stations is extremely differ from other months TEC value. This is because March and April months are parts of equinoxes while February is Winter season. As it is known and very well depicted in the Fig. 5.10 the value of TEC is maximum during the equinoctial and winter seasons as compared to summer season.

From TEC versus Universal time curve we deduce that TEC does not suddenly disappear, but gradually increasing and decreasing before 0600 and after 1600 UT respectively. From these temporal and diurnal variation of TEC, one can infer that the change comes from the Sun's activities such as sun spot number and solar flares which often accompany the fast coronal mass ejection and geomagnetic activity variation. The day-to-day or month-to-month variability in TEC, which has also been observed by some authors [49, 50], may be due to the changes in the activity of the Sun itself and

to the associated changes in the intensity of the incoming radiations and the zenith angle at which they are incident on the Earth's atmosphere. Generally this temporal variation depends on the intensity of radiation comes from the Sun since intensity is increasing beginning from sunrise and reaches maximum after Sun is overhead 1 hr later and also decreasing late afternoon and comes to zero when sunset at about 2300 UT or 0000 UT. The reason for this phenomenon is that the hourly values of TEC can be altered by intensity of solar electromagnetic radiation and emission of particles from the Sun.

5.4 Seasonal Variation of Ionospheric TEC

To study the seasonal variability of the ionospheric TEC, Lloyd's seasons [51, 52], in which the whole year is allotted in to three seasons; December or D-season (December, November, January and February), Equinox or E-season (March, April, September and October) and June Solstice or J-season (May, June, July and August) are used.

During Equinox the Sun shines directly on the equator and the length of day and night is nearly equal and because of maximum photo-ionization, maximum TEC in the equatorial ionosphere is expected. It is important to note that Earth does not move at a constant speed in its elliptical orbit. Therefore the seasons are not of equal length: the time taken for the Sun to move from the vernal equinox to the summer solstice, to the autumnal equinox, to the winter solstice, and back to the vernal equinox are roughly 92.8, 93.6, 89.8 and 89.0 days respectively.

The consolation in the northern hemisphere is that spring and summer last longer than autumn and winter (when the December solstice occurs). The relative position of the Earth's axis to the Sun changes during the cycle of seasons. This phenomenon

is the reason why the Sun's height above the horizon changes throughout the year. It is also responsible for the seasons through controlling the intensity and duration of sunlight received at various locations around the planet. So during solstice the Sun is not overhead at the equator, that means the light intensity that pass through the ionosphere above the equator is small compared to the equinox which leads to small value of TEC in the ionosphere which in turn produces different navigational and communication problems.

Accordingly, the occurrence time of the maximum/minimum ionospheric TEC values varies with seasons. The seasonal variation of ionospheric TEC for Addis Ababa (9.04^0 N, 38.77^0 E) and Bahir Dar (11.6^0 N, 37.36^0 E) stations since 2015 is stated in Fig 5.10. The study of TEC variation at both stations have been grouped into three seasons as in the case stated before. Fig 5.10 shows the variation of TEC for the whole seasons for the two stations. As observed from this Fig., the TEC variations attained maximum during the afternoon with equinoctial months followed by winter for the two stations. Summer months recorded the least TEC amplitudes in both Addis Ababa and Bahir Dar.

In general, the morning rise to peak in the afternoon and then fall in TEC was sharp during the equinoctial months. Also, the production of O/N_2 was faster in winter than in summer. These could be explained using thermospheric neutral composition. Thermospheric neutral composition has a direct control on the seasonal variation of TEC. Rishbeth and Setty [53] suggested that the seasonal changes result from changes in ratio of the concentration of atomic oxygen and molecular nitrogen in the F-region. During the daytime, the equator is hotter than the pole, therefore meridional wind flows towards the pole from the equator. This flow of meridional

wind changes the neutral composition and O/N_2 decreases at equatorial and low latitude stations. The decrease is maxima in equinoctial months. At 350 km altitude (F2-layer), N_2 dissociation is the major process which removes ambient electrons. Hence, the decrease in O/N_2 ratio will result in higher electron density and therefore in equinox, TEC will be highest.

The Sun is overhead at the equator around the time of the equinoxes. This seasonal cycle causes a corresponding seasonal and spatial variation in the global ionospheric structure. The D, E and F1 region electron densities are greater in summer than in winter. However, the variation in F2 region electron densities is more complicated. In both hemispheres, electron densities generally peak around the equinoxes [31]. Around solar minimum the summer noon electron densities are, as expected, generally greater than those in winter, but around solar maximum winter frequencies tend to be higher than those in summer a phenomenon called seasonal anomaly [32].

During summer, the Sun changes its position to Northern hemisphere since Ethiopia is found in Northern hemisphere maximum solar radiation intensity reaches on its atmosphere. During this time the neutral wind flow from north to south Pole, for this reason minimum TEC value is recorded at the two stations under investigation of study found in Ethiopia. During winter season the Sun changes its position to Southern hemisphere while Ethiopia is found in Northern hemisphere and near to equator during this time medium radiation reach on its atmosphere and TEC value recorded during this time is also medium. This is because the Sun shines directly on the equator and causes high ionization during September and march equinox but the Earth becomes tilted towards or away during solstice caused to decrease the emission of solar radiation to the Earth's ionosphere.

The position of the Sun relative to the equator affects the ionization process in the ionosphere because the intensity of ionization depends on the solar zenith angle. That is when the sun is at different positions the solar zenith angle changes so the rate of production will be changed. When the Sun is at horizon the intensity reaching the equatorial ionosphere is relatively small compared to the intensity reaching at the equatorial ionosphere from the overhead Sun. The results of variation in median TEC over the low-latitude stations considered in this study showed that the variation of median TEC is dependent on seasons and local time of occurrence in both stations of Ethiopian low latitude regions. As shown in Fig. 5.11 in the whole seasons the maximum value of TEC leads first in Addis Ababa followed by Bahir Dar. The difference in VTEC over Addis Ababa and Bahir Dar is due to differences in geographical latitude.

5.5 Solar activity dependence of TEC

The Sun emits a wide spectrum of radiation along with high energy particles. We know, radiation is absorbed and intensity is decreased. If intensity were not decreased or radiation were not absorbed one cannot exist over the Earth. This radiation increases during high solar activity and this has its own effect on Earth's ionospheric TEC, the leading indicator of Space Weather. To see the effect of this solar activity on the GPS-TEC, we demonstrate the solar activity indices (sunspot number and radio flux) data.

As can be seen from top panel of Fig. 5.12, the number of sunspots and solar flux changes with an 11-years period which is called the solar-activity cycle (solar cycle) as observed on Fig. 5.12. The demonstrated year 2015 is found around peak of solar

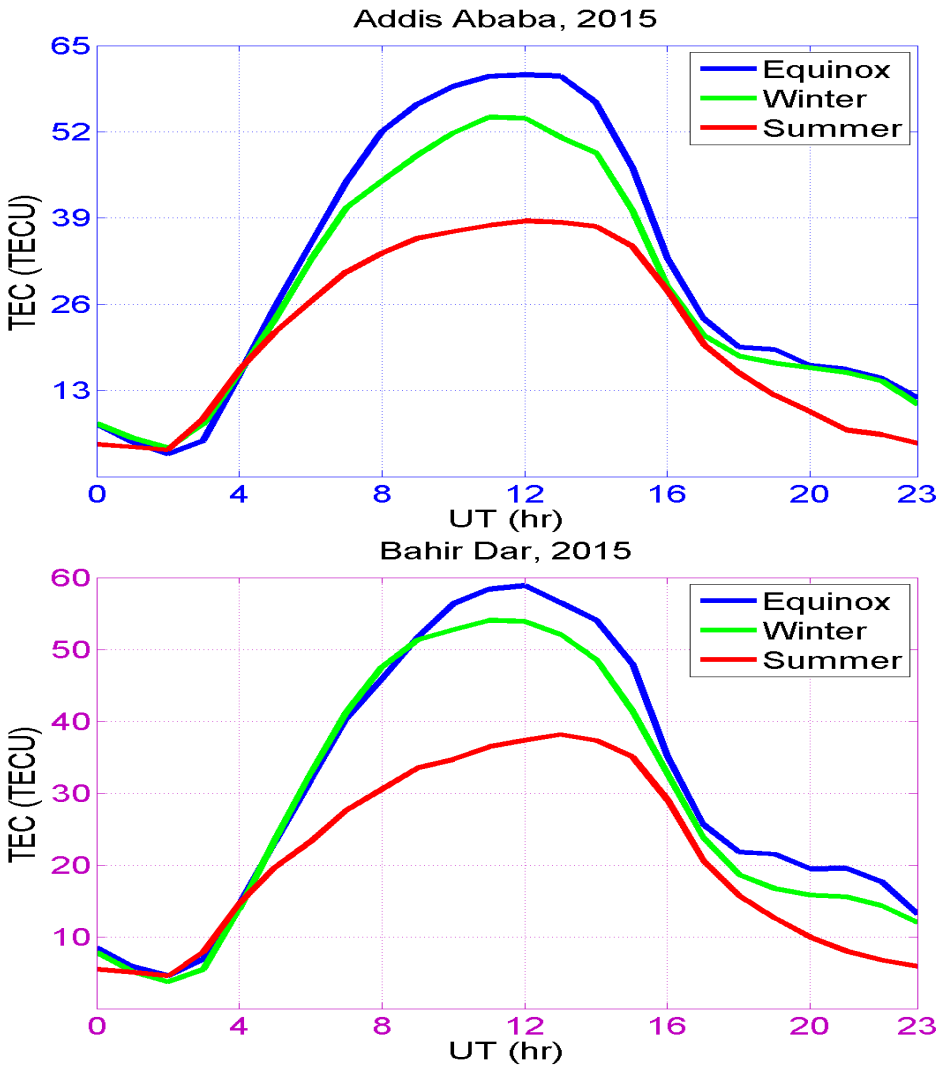

Figure 5.10: The median seasonal Variation of TEC observed at Addis Ababa and Bahir Dar Stations during 2015.

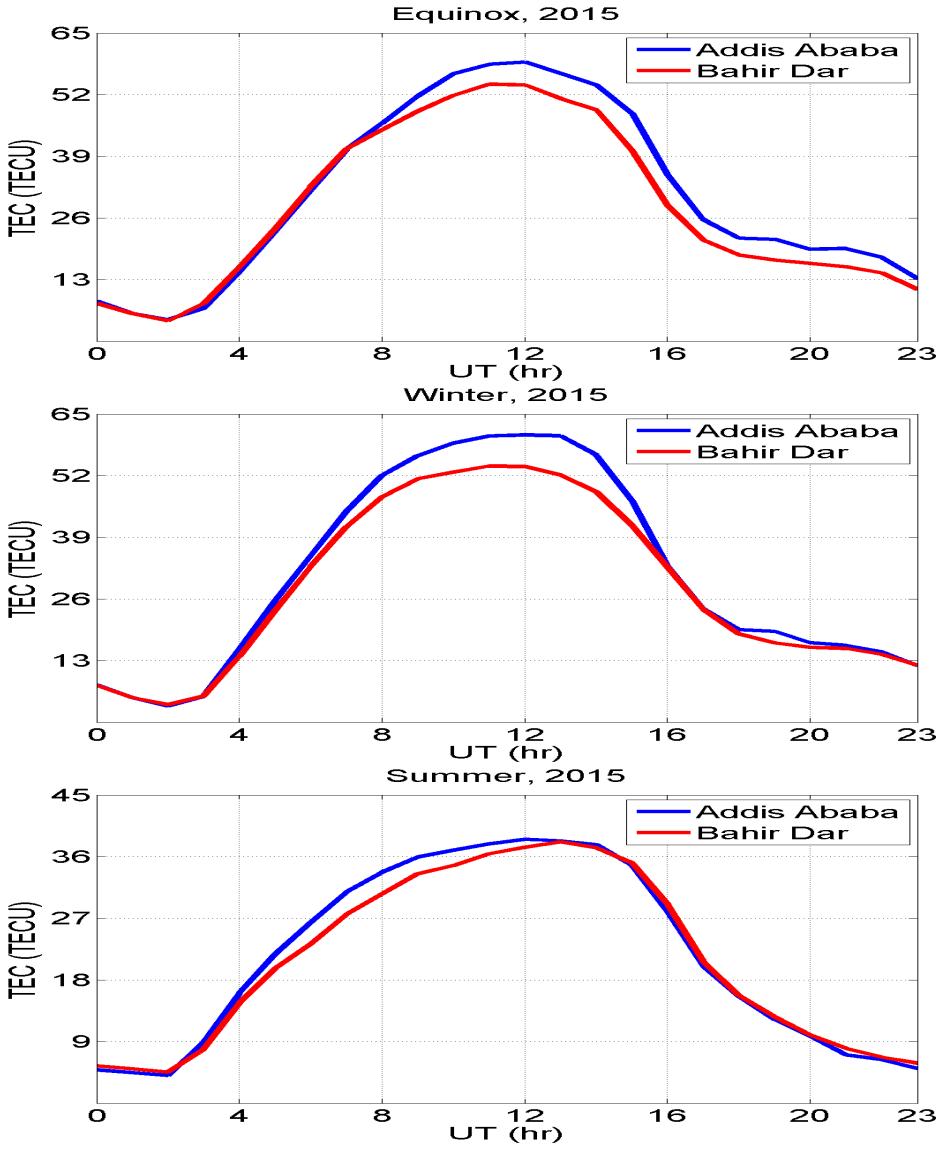

Figure 5.11: The dependence of seasonal variation of TEC on location.

cycle 24 as shown in Fig 5.12 by red arrow. The peak of this solar cycle is indicated by the blue arrow on the stated Fig. which is 2014.

Today we know that all solar activity phenomena are related to sunspots and thus to magnetic activity. Along with the sunspot number, the flux of the Sun's radio emission at a wavelength of 10.7 cm (2.8 GHz) is a useful indicator of solar activity relevant for ionospheric effect. Solar flux from the entire solar disk at a frequency of 2800 MHz has been recorded by a radio telescope near Ottawa since February, 1947 [54]. The other quantity to take into account is the precipitation of particles most of them coming from the Sun (CMEs). The sunspot number index is also often called Wolf number in reference to the Swiss astronomer J. R. Wolf who introduced this index in 1848 [54]; sunspots and the solar-cycle. The Sunspot is annual, diurnal and monthly variable physical quantity which is expressed in terms of number. Both sunspots and solar radio flux are indicators of solar activity for ionospheric ionization level, with higher value during maximum solar activity and low value during minimum solar activity.

Ionosphere is not a stable medium that allows the use of the same frequency throughout the year, or even over 24 hours. It varies with the solar cycle, the seasons and during any given day. These solar activities have their own effects on the total electron content (TEC) (principal indicator of ionospheric variability). As observed from Fig. 5.12 (Middle) and (bottom) panels of area graphs in the year of investigation 2015, in general it was found that the sunspot number and solar radio flux are directly proportional to each other.

Now let us investigate how TEC is affected by sunspot number and solar radio flux. Figs. 5.13 to 5.16, demonstrates daily average sunspot numbers and Sun's radio

emission at a wavelength $\lambda = 10.7$ cm and frequency $\nu = 2.8$ GHz. Fig. 5.13, shows around the beginning of January 11, both sunspot number, radio flux and TEC have higher magnitude and fall down together around January 16, 2015. Again from January $16 - 25$ both the sunspot number and solar radio flux shows moderate values. After January 26, both sunspot number and solar flux increases to maximum and medium values respectively. Similar phenomena has occurred before January 11. Here we can see that the value of TEC also increases and decreases in line with the values of these parameters on those corresponding days as depicted from the contour plot.

So far we have seen that TEC is maximum on March 30 (doy = 80), 2015 next to April 3 (doy = 93) and February 9 (doy = 40) with magnitude of 79.27 TECU in Bahir Dar station. From Fig. 5.14, we have seen that as sunspot number and solar flux are both increased together on March 30 and in the same corresponding days the TEC also increased. We have seen maximum TEC value during March, 2015 and during this time the sunspot number and solar radio flux are fair but there are geomagnetic storms during this month. We will see effects of geomagnetic storm days in this month and other similar geomagnetic storm days on other months on the next section.

Fig. 5.15, shows from May $10 - 15$ both sunspot number, radio flux and TEC have great magnitude together and fall down between May 20 and 30, 2015. Similar with the previous days of months, during August 2015 the variation of TEC in line with the solar activity indices also observed. In general from Figs. 5.15 to 5.16, maximum TEC value is formed during spotted day while minimum TEC value is formed during spotless days. For the day exhibits maximum sunspot numbers and solar radio flux

the TEC value is also maximum. It is highly relevant for ionospheric effects. Rao et al.(1985) [55] reported the direct control of the solar activity on the ionization level, with higher values during a high solar activity period and low value during a low solar activity period.

From the whole Figs. (5.13−5.16) we deduce that, during the period of low or high sunspot number, the provided GPS ionospheric TEC builds up slowly or quickly. This result has a positive agreement with a study by Warnant et al. and Amensisa et al. [48, 55].

5.6 Variation of TEC during geomagnetic storms

The Earth's ionosphere responds dramatically to geomagnetic storms coupling the neutral thermosphere with the overlying magnetosphere. During the sever geomagnetic storms penetrating electric fields and plasma redistribution combine to produce enhancements and reduction of ionospheric TEC, steep localize density gradients and storm time Space Weather effects. Ionospheric measurements often indicate that during magnetically disturbed conditions the low latitude electric fields and currents are largely depart from their quiet time averages ([56] and references therein). The direct penetration of the high latitude electric field to the lower latitude and the ionospheric disturbance dynamo are the two major contributors to the ionospheric electric field at low latitude during geomagnetic disturbances [57, 58].

Geomagnetic disturbances are caused either when the interplanetary magnetic field (IMF) is directed south ward or when the magnetosphere of the Earth is stroked by solar wind. Interplanetary electric fields, caused by the convection motion of the solar wind across the interplanetary magnetic field as inferred from $\vec{E} = \vec{v} \times \vec{B}$ ([59]

and references therein), may appear almost immediately in the Earth's magnetosphere and ionosphere after these electric fields are convicted from the solar wind to the magnetosphere. This phenomenon is commonly termed as the prompt penetration of the interplanetary electric field (IEF) in to the magnetosphere/ionosphere system, or simply electric field penetration.

In this topic we tried to analyze the observed events on June starting from June $21 - 23$, 2015. A severe storm occurred on June $21 - 23$, 2015. The storms arose in response to variable solar-wind conditions that the Space Weather Prediction Center of the National Oceanic and Atmospheric Administration (SWPC, NOAA) associated with active region on the Sun. The National Aeronautics and Space Adminstration's (NASA's) SOHO detected series of 3 coronal mass ejections (CMEs) originated from this active region. These were subsequently recorded by NASA's Advanced Composition Explorer (ACE) satellite, located on the Sun-Earth line at a distance approximately 1% of the distance from the Earth to the Sun, as abrupt enhancements in solar-wind velocity and density. With the arrival of the CMEs at the Earth on about June 21 at 16:45 UT, June 22 at 05:45 UT, and June 22 at 18:30 UT, concomitant increases in solar-wind ram pressure abruptly compressed the Earth's magnetosphere. This storm saw a maximum Dst of -195 nT, realized on June 23 at about 04:30 UT and -204 nT at about 5000 UT and, so, by this measure this storm was slightly smaller than the storm of March 17, 2015. Still, this storm is the second largest of this unusually subdued solar cycle.

Following a Coronal Mass Ejections (CMEs) on 21 and 22 June 2015, we have observed the pre, during and the post events by using solar wind parameters. Geomagnetic activity is caused by transfer of energy and momentum from solar wind to

the magnetosphere that occurs in response to the southward interplanetary magnetic field. The geomagnetic storm that have occurred during June 23, 2015 is characterized using observational data analysis such as the variation of the $SYM - H$, $ASY - H$, AE, V_p, IMF B_z, proton temperature and density, flow pressure, and proton flux events. Previous studies have used these parameters in part or in whole to characterize the nature of geomagnetic storms. For instance, large number of studies have associated geomagnetic storms with extreme increase in the solar wind velocity and/or southward interplanetary magnetic field (IMF) due to coronal mass ejection (CME) and their associated interplanetary shocks.

Fig. 5.17 (top) panel shows $SYM - H$ over a period of selected 20 days that includes few days before and after the occurrence of the storm. It is a high resolution since it has a temporal resolution of a minute and can be regarded as a high resolution Dst index. As shown in Fig. 5.17, the $SYM - H$ value on June 21 at 16:45 UT, June 22 at 05:45 UT, and June 22 at 18:30 UT shows a sudden increase to more than 50 nT at the sudden storm commencements (SSC)s and then sharp decrease to a value of -204 nT after which a recovering starts followed by another shock on June 23. The compression exerted on the sunward side of the Earth's magnetosphere by strong plasma cloud (CMCs) ejected from the sun is responsible to develop sudden storm commencement (SSC) and main phase of the storm. These SSCs before the main storm on June 23 are evidences for the occurrence of Coronal Mass Ejection (CME) which causes compression of the magnetosphere leading to fluctuation of the Earth's magnetic field.

It is known that geomagnetic storms can also be driven by Corotating interaction regions (CIRs). However, the storm that have happened on June 23, 2015 is likely to

be due to the CME because the recovery period is short unlike that of CIR driven geomagnetic storms. The $SYM-H$ value shows a sharp positive increase more than 50 nT which is a SSC before the main storm phase indicating a fast forward shock is formed. When geomagnetic storm occurs the $Dst < 0$ because there exists enough reconnection to sufficiently energize the ring current to overcome the preexisting huge magnetopause current. A fall in the $SYM-H$ index is typically accompanied by the plasma sheet moving inward of geosynchronous orbit, with the highest increase in the ion and electron densities occurring during the main phase of the storm at, or close to, minimum $SYM-H$ index value.

Another geomagnetic disturbance index is the $ASY-H$ index which is a measure of the difference between the maximum and minimum $SYM-H$ values. Fig. 5.17, middle panel, shows that on day 23 the difference between maximum and minimum $SYM-H$ values is exceptionally large compared to the other undisturbed days. Fig. 5.17, bottom panel, shows enhancement in AE index on day 23. This index is particularly suitable to characterize the polar region. The high values on this date implies ionospheric perturbation. This is an indication of significant amount of energy was injected at high latitude during the storm period in contrast to the geomagnetically quiet days whose AE index value is significantly small.

The sudden jump of the solar wind dynamic pressure in Fig. 5.18, top panel, and the IMF B_z in Fig. 5.18, middle panel, corresponding to the bow shock called magnetic storm sudden commencement clearly are other indicators that the storm is driven by CME. As indicated in the Fig. 5.18 (top panel) a sharp enhancement of flow pressure on June 23 followed by falling into its normal value on the rest days is another evidence of CME driven storm. Fig. 5.18 (middle) represents IMF B_z

during the 20 days period encompassing the storm time and depicts the behavior of the IMF B_z before, during and after the occurrence of geomagnetic storm. The IMF B_z value during the quiet days was almost zero but sharply and momentarily increases signalling the onset of the storm after which it falls into its negative value until it reaches the end of the main phase of the storm. The reason for this event is, when the IMF B_z and geomagnetic field lines are oriented opposite or anti-parallel to each other a bow shock occurs and they can merge or reconnect resulting in the transfer of energy, mass and momentum from the solar-wind flow to magnetosphere and then the magnetosphere effectively opened up to the solar wind, allowing electrically charged, energetic particles to be deposited into the inner magnetosphere.

The IMF B_z is not highly variable except at the fast forward shock which suggests that the geomagnetic storm is $CME-$driven. This is in agreement with other indices so far discussed. In the case of southward B_z, more energy deposition into the higher ionospheric latitudes is observed due to the possible magnetic reconnection processes. The dawn-to-dusk disturbance electric field in the equatorial ionosphere is associated with southward turning of the interplanetary magnetic field component, B_z ([60] and references therein). The southward interplanetary magnetic field and the continuous increase of AE activity that recovers its original shape after IMF B_z turns north imply the pre storm and post storm conditions have the same phenomena.

Lindsay et al [61] and many other investigators have demonstrated that geomagnetic storms are accompanied by high solar wind velocities, and enhanced solar wind dynamic pressure and CME. The southward solar wind velocity in Fig. 5.18, bottom panel, reaches $-43\ \frac{m}{s}$ on June 21, $-55\ \frac{m}{s}$ on June 22 followed by another maximum speed of about $-179\ \frac{m}{s}$ on June 23 accompanied by recovery on June 24. These

features in the solar wind velocity confirm previous indicators that three CME are responsible for the geomagnetic storm.

The huge enhancement of the proton density in Fig. 5.19 (top panel) on June 23, 2015 also is an indicator for the deposition of solar materials as a result of CME that has happened on that day. The ion density enhancement at time of minimum Dst appears to be directly related to the magnitude of the Dst with larger densities during the larger storm due to CMCs [4]. Comparison of proton density during the 20 days time series show that its value during June 23 is greater than other geomagnetic stormless and weak stormy days. Fig. 5.19 (middle panel) shows maximum proton temperature on June 23 which is consistent with the proton flux and energy category in contrast to the temperature during the rest of observation periods.

Fig. 5.19, bottom panel, shows the east west electric field estimated from $\vec{v} \times \vec{B}$. It is clearly evident that there is prompt penetration electric field during the disturbed days. Basically the interplanetary southward magnetic field's component (B_z) introduces a dawn-to-dusk interplanetary electric field (IEF) at the magnetopause given by $E_y = -\vec{v_{sw}} \times \vec{B_z}$ so that during the time interval between connection and reconnection of geomagnetic field lines are open and IEF can penetrate to the polar regions of the ionosphere causing sudden changes in cross cap. This electric field can be instantaneously mapped to the lower latitudes to change the lower ionosphere dynamics [62].

A solar proton event (SPE) occurs when protons emitted by the Sun become accelerated to very high energies during a solar flare accompanied by a CME or in interplanetary space by the shocks associated with CMEs. Protons are finally guided by the interplanetary magnetic field lines. As observed from Fig. 5.20, the energy of

$E > 10$ MeV, proton flux is nearly 1040 pfu (1 pfu=1 particle flux unit) following the storm on June 23 and very much negligible after the one on June 24, 2015. Similarly, for $E > 30$ MeV energy range, proton is more than 10 pfu on day 23, 2015 while the proton flux with energy $E > 60$ MeV, is more than 0.32 pfu for the SSC. These high energy proton flux can produce abnormal ionization in the lower ionosphere that is visible in the TEC enhancement as shown under this section.

Once we have analyzed the geomagnetic storm occurred during June 23, 2015 let's look the effect of this geomagnetic storm and other months disturbed days effect on TEC values. On sunspotted day more solar electromagnetic radiation and energetic particles such as CME, solar flare, X-ray, EUV are bombarding the ionosphere to have large magnitude of TEC. Strong solar flares could be, associated with cosmic ray and it disrupts radio communication on Earth, the intense X-ray and EUV radiation emitted during the flares heats the atmosphere, disrupting communication and altering Satellites orbits [63].

The size of a geomagnetic storm is classified as moderate when Dst is between -50 nT and -100 nT, intense storm between -100 nT and -250 nT and super storm below -250 nT. Super storms have an annual variation, with higher occurrence around the equinoxes. Most of super storms have a short main phase duration $(10 - 20)$ hr. But there are cases more complex, with main phase lasting more than 40 hours [55]. The Ap is computed every 24 hrs and during quiet periods just above zero but may rise up to 400. $0 < Ap < 10$ nT shows no disturbance and $Ap > 10$ nT shows there is a geomagnetic disturbance.

From Figs. 5.21 to 5.24 maximum TEC on day March 17 and 18 with Dst value of -222 nT and -189 nT respectively around equinox, June 23 and August 27 with Dst

value of -204 nT and -92 nT respectively around summer solstice and November 10 with Dst -58 nT at 1400 UT during winter solstice occurred during the main phase of the geomagnetic storm. The Dst values measured on March $17-18$ and June 23 shows us there are intense geomagnetic disturbance and moderate during August 27 and November 10.

As can be seen from Fig. 25, several types of geomagnetic storms occurred and even with minor geomagnetic storm levels for the corresponding days. The effect of a geomagnetic storm on the ionospheric TEC has been studied by many researchers. The geomagnetic activities have both negative and positive storm effect. The TEC response to the storm depends on the universal time of sudden storm commencement (SSC). In the case of a day time SSC storm, a prompt penetration electric field directed east ward raises low latitude plasma upward due to the $\vec{v} \times \vec{B}$ drift where the recombination rate is slow. An increase in the electrodynamics drift will lift more plasma from equatorial region which diffuses down along the field lines to higher latitude and result in the increase of the TEC at stations under the anomaly crest region [59, 64].

From Fig. 25, the value of TEC observed at June 23, 2015 was high relative to other undisturbed days in the month. This phenomenon of the TEC variation comes due to SSC in the day local time, in which the high value of interplanetary geomagnetism recorded from this particular day (June 23) and the other months of disturbed days of 2015 as really supported by Ap index bar graph.

As shown on Fig. 25 there are different kinds of SSCs of geomagnetic storms. From this different SSC we took some days from international disturbed and undisturbed

days at which strong geomagnetic storm is formed and no geomagnetic storm was happened respectively depending on Dst indices. International Quiet Days (IQD's) are the days where the geomagnetic variations are minimum in each month. International Disturbed Days (IDD's) are 5 days in each month where the geomagnetic variations are maximum. The classification of days is relative only to the month of calculation. The average disturbance level in one month may differ from another. Diurnal and disturbance-dependent change in the ionospheric TEC depends on Space Weather. Therefore, there is strong relationship between geomagnetic storm and variation in the ionospheric TEC.

Fig. 5.26 shows TEC values during IDD's and IQD's at Bahir Dar station during 2015. In these Figs. X-axes shows hours universal Time (UT) and Y-axes shows TEC values in TECU. The red lines in the Fig. 5.26 depict TEC values obtained during disturbed days while the blue lines depict TEC values obtained during undisturbed days. During June and August the TEC value on disturbed days is greater than the TEC value on undisturbed days. The TEC values on disturbed days of June 23 (doy = 174) and August 27 (doy = 239) are 42.21 TECU at 1400 UT and 46.8 TECU at 1500 UT respectively while on undisturbed days of June 20 (doy = 171) and August 14 (doy = 226) are 30.89 TECU at 1400 UT and 33.90 TECU at 1400 UT. The maximum values in TEC during November 10 (doy = 314), is 55.68 TECU at 1100 UT but during November 24 (doy = 328), 47.17 TECU at 1300 UT.

Similar with June and August the TEC value during November 10 (doy = 314) is greater than that of November 24 (doy = 328). Here we observe that TEC value changes irregularly for disturbed days as compared to undisturbed days. The maximum values in TEC during March 10 (doy = 69), is 65.14 TECU at 1200 UT but

during March 17 (doy = 76), 63.96 TECU at 1200 UT. Contrary to the aforementioned days of months result, the value of TEC during March 10 (doy = 69) is greater than that of March 17 (doy = 76).

In Addis Ababa station as shown in Fig. 5.27 due to the in availability of the data on the corresponding days of observation like on Bahir Dar station on March, August and November, we selected the next IQD's and IDD's on these days of months by keeping the phenomena on June as already done by that day due to the data availability. Here also the red lines depict disturbed days while blue lines depict undisturbed days. As observed here the value of TEC on August 23 and June 20 is greater than June 20 and August 24 respectively. The value of TEC on March 30 and November 25 is greater than March 18 and November 7, respectively.

Generally we observe that the value of TEC is maximum during disturbed days as compared to undisturbed once. In a different case the value of TEC is maximum on undisturbed days of March $17-18$ and November 25, 2015 as compared to disturbed days as observed from the study areas found in Ethiopia, East Africa. Geomagnetic storms may be positive or negative in regarding to their effects on TEC, that is the value of TEC increases due to positive while decreasing due to negative geomagnetic storms. So we showed that the storms occurred during March $17-18$ and November 25 are negative storms while the rest days of geomagnetic storms are positive storms since they increase the value of TEC as compared to other undisturbed days of the observed months. When TEC is maximized/minimized by storms in the ionosphere the radio communication will also be disrupted. In all aspects of observation we saw that the variation of TEC of the ionosphere results due to Space Weather effects.

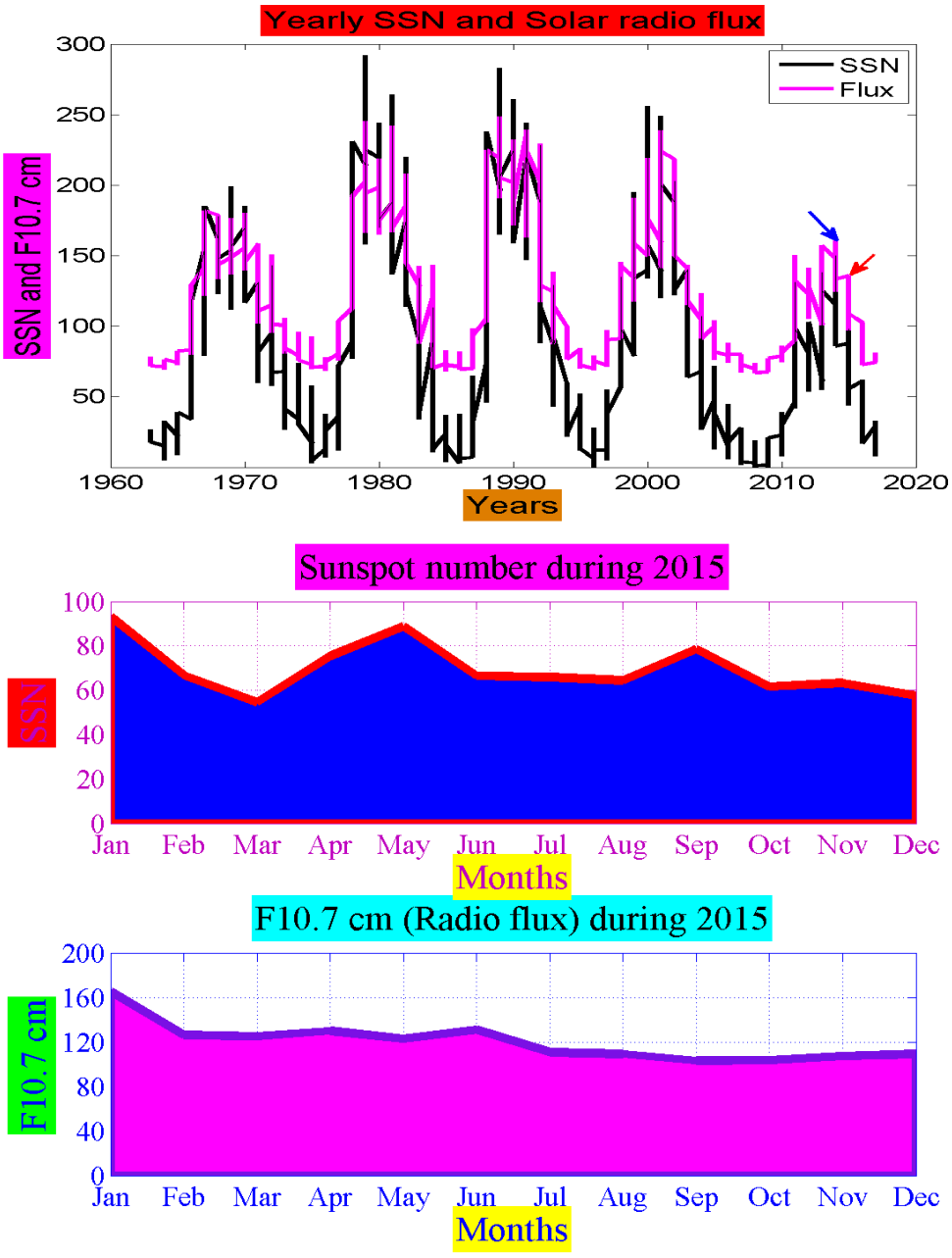

Figure 5.12: Sunspot number and solar radio flux during (1963 – 2017) (top), sunspot number during 2015 (Middle) and Solar radio flux (bottom) in 2015.

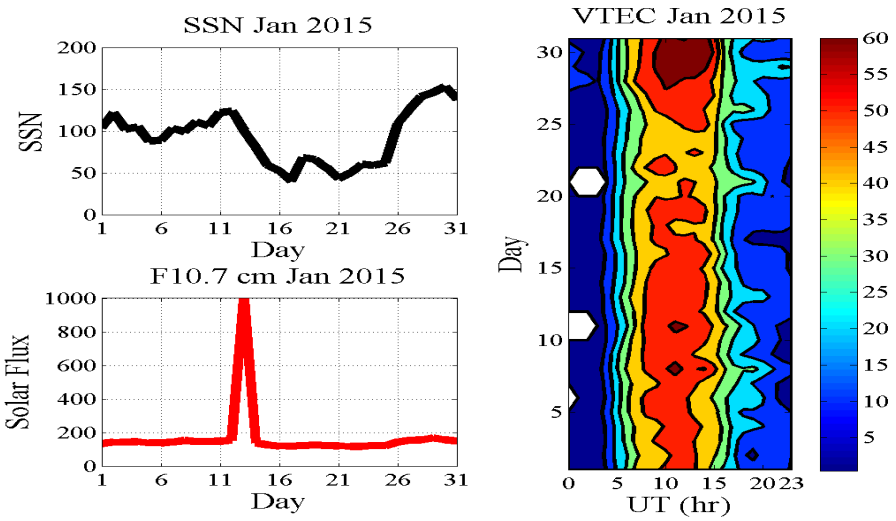

Figure 5.13: Sunspot number, Solar radio flux and VTEC during January of 2015.

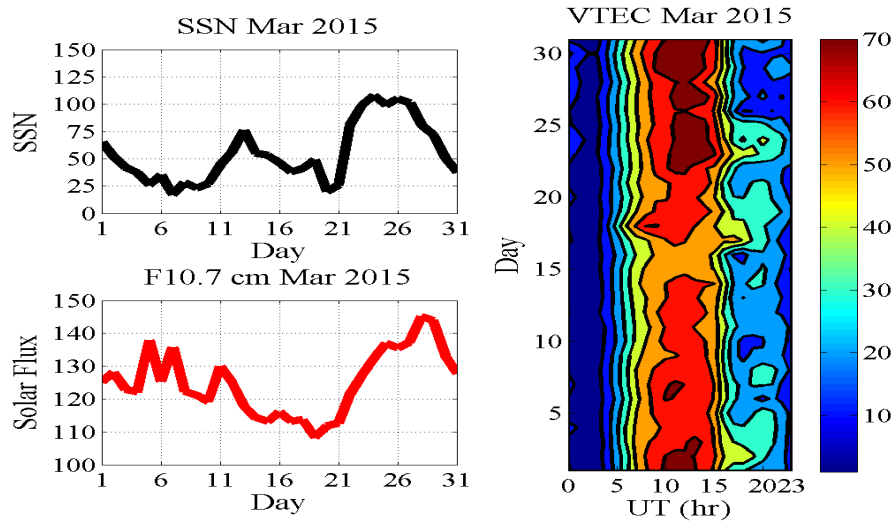

Figure 5.14: Sunspot number, Solar radio flux and VTEC during March of 2015.

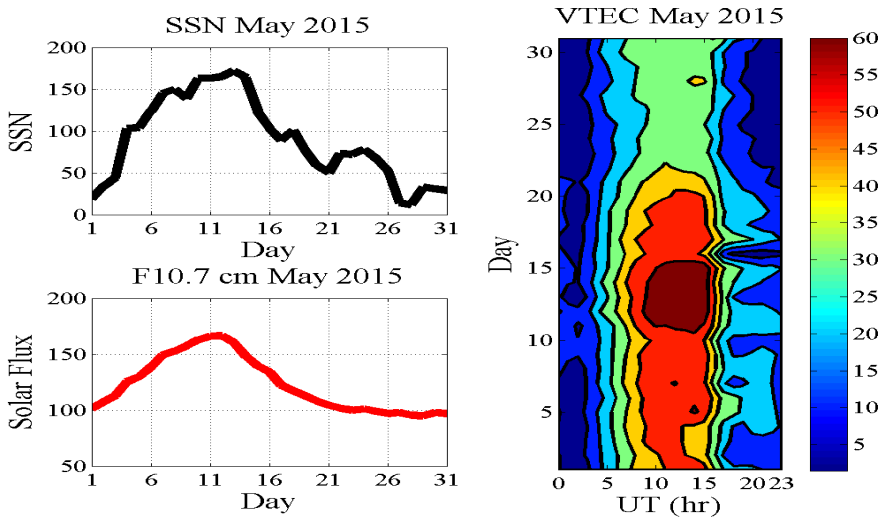

Figure 5.15: Sunspot number, Solar radio flux and VTEC during May of 2015.

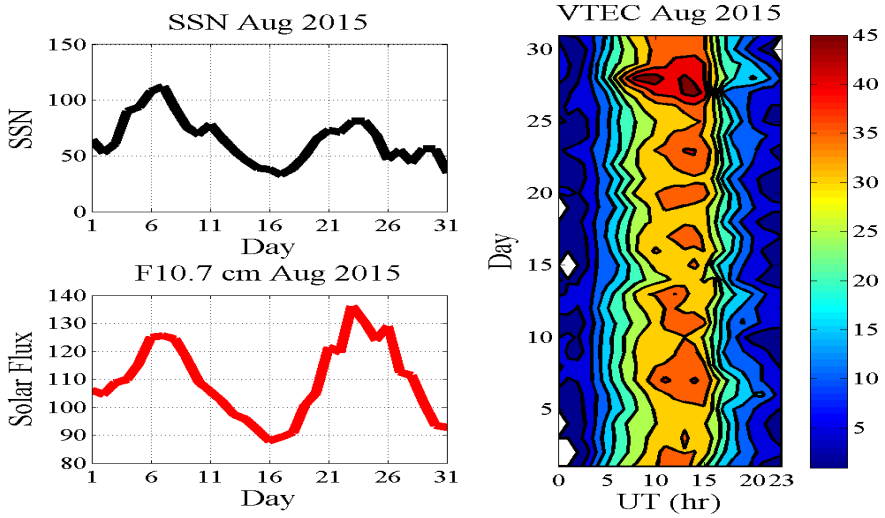

Figure 5.16: Sunspot number, Solar radio flux and VTEC during August of 2015.

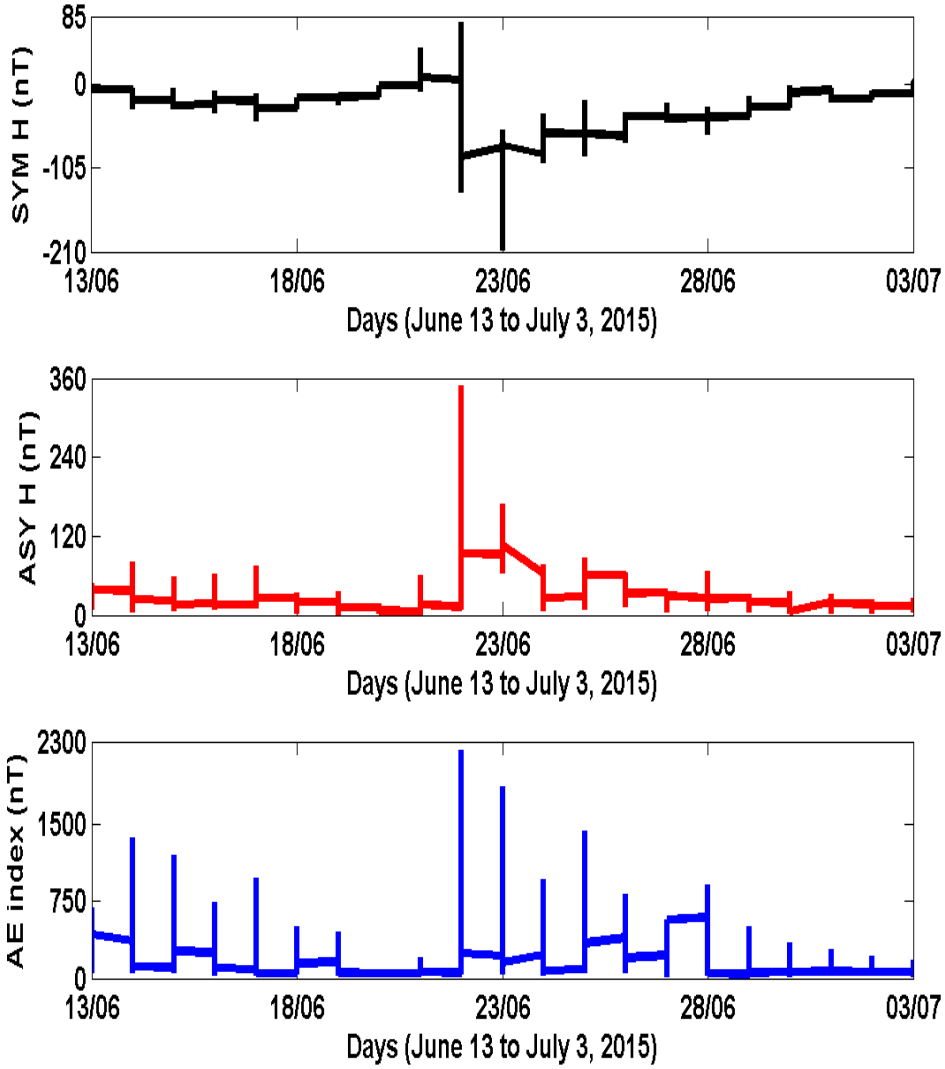

Figure 5.17: $SYM-H$, $ASY-H$ and AE index time series during June 13−July 3, 2015.

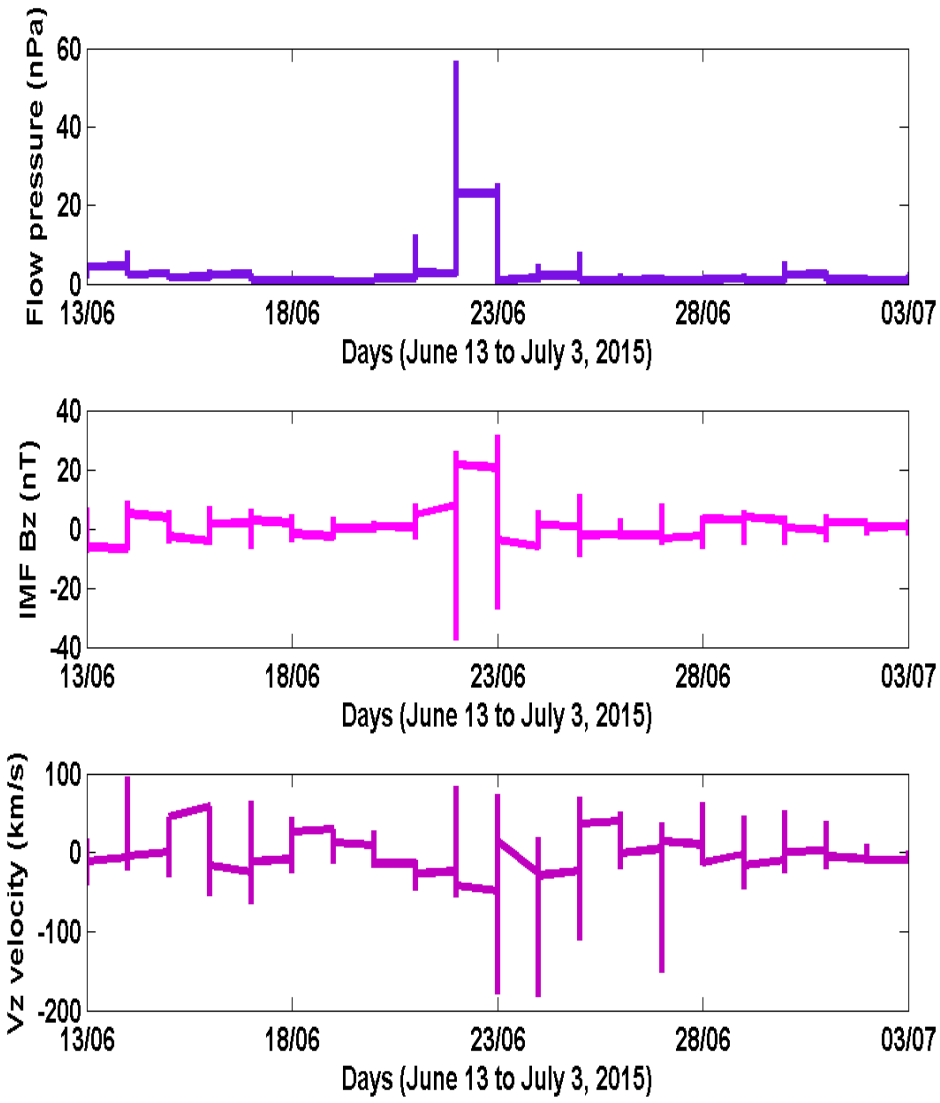

Figure 5.18: The variation of solar wind dynamic pressure in nPa (top), IMF B_z (middle) and solar wind velocity (bottom) during June 13−July 3, 2015.

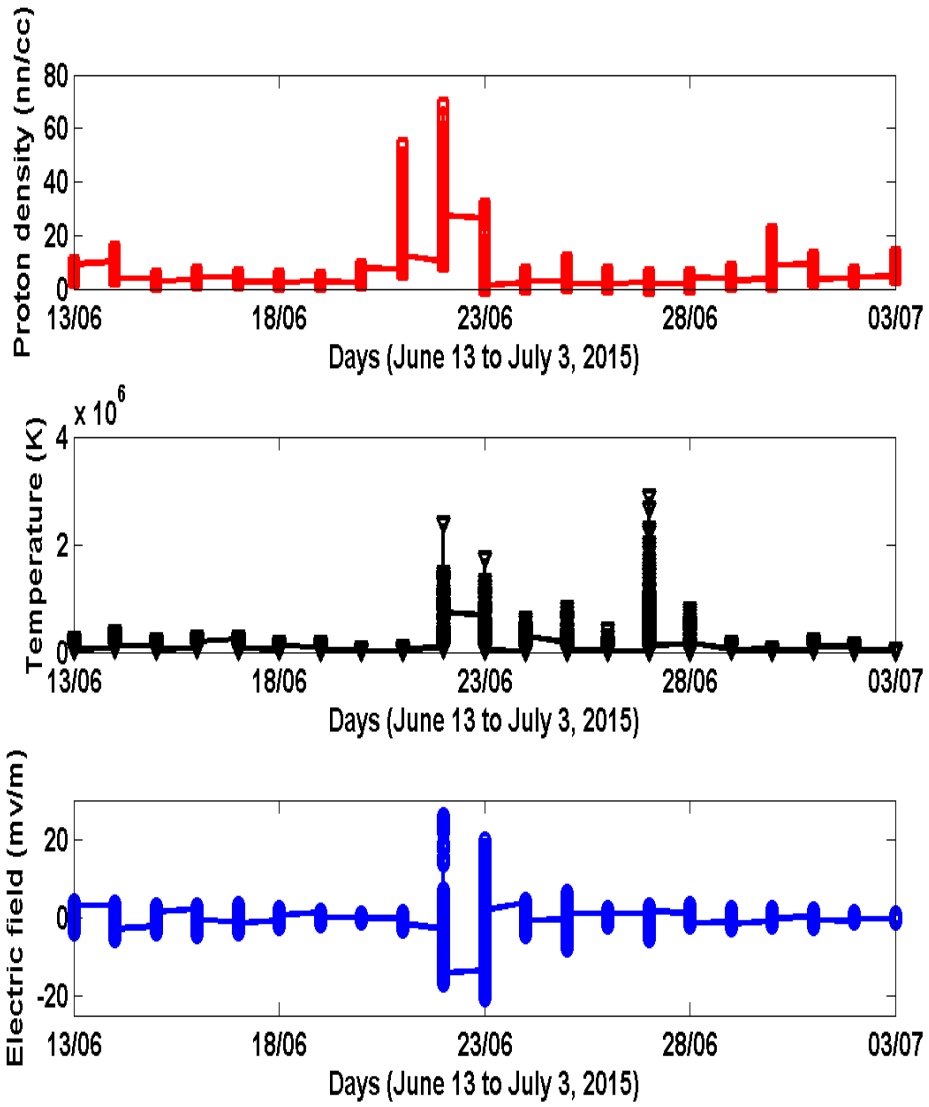

Figure 5.19: Proton density in nn/CC, temperature and derived electric field during June 13– July 3, 2015.

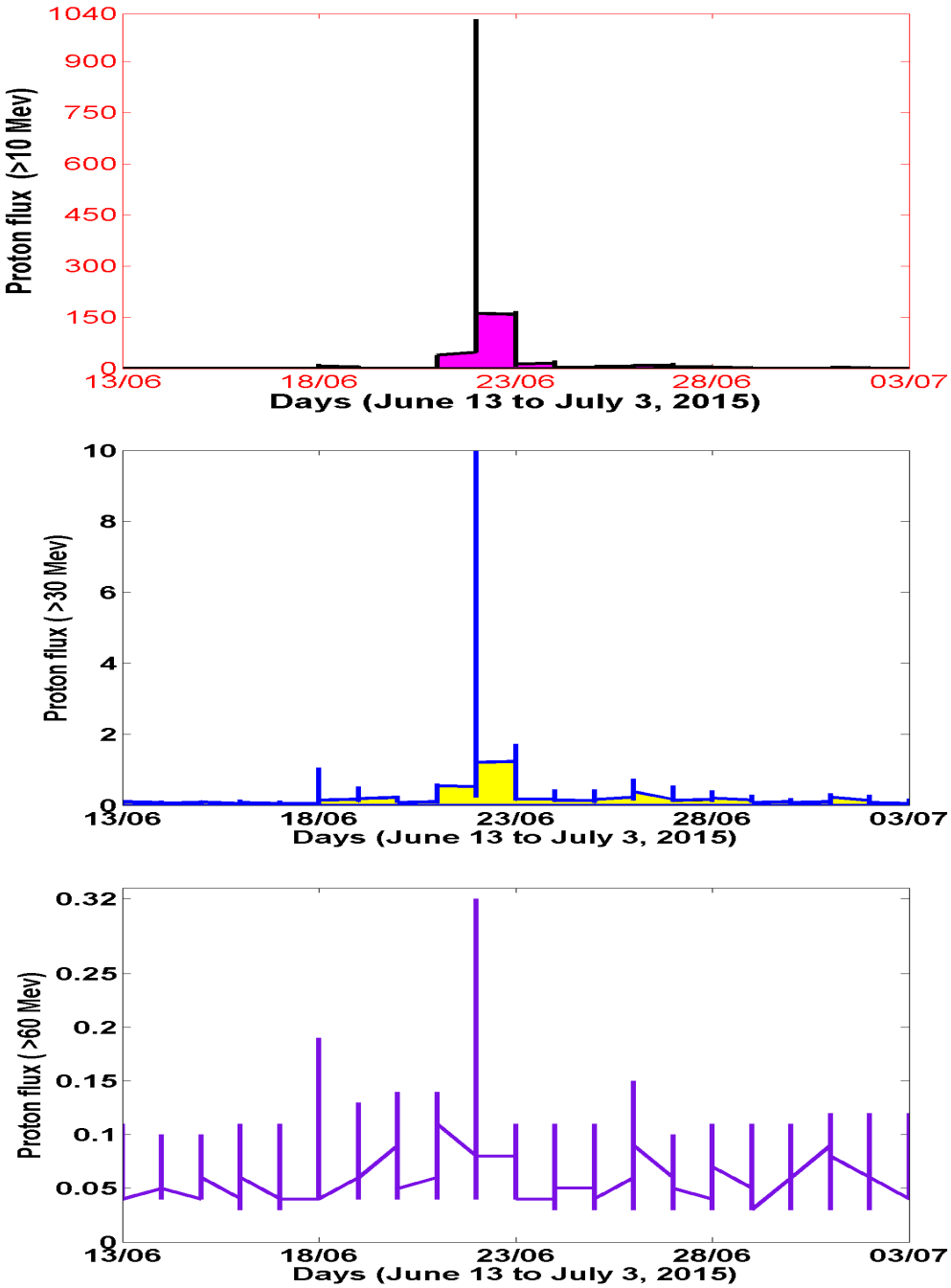

Figure 5.20: Proton flux ($>$ 10 Mev), Proton flux ($>$ 30 Mev) and Proton flux ($>$ 60 Mev) during June 13$-$July 3, 2015.

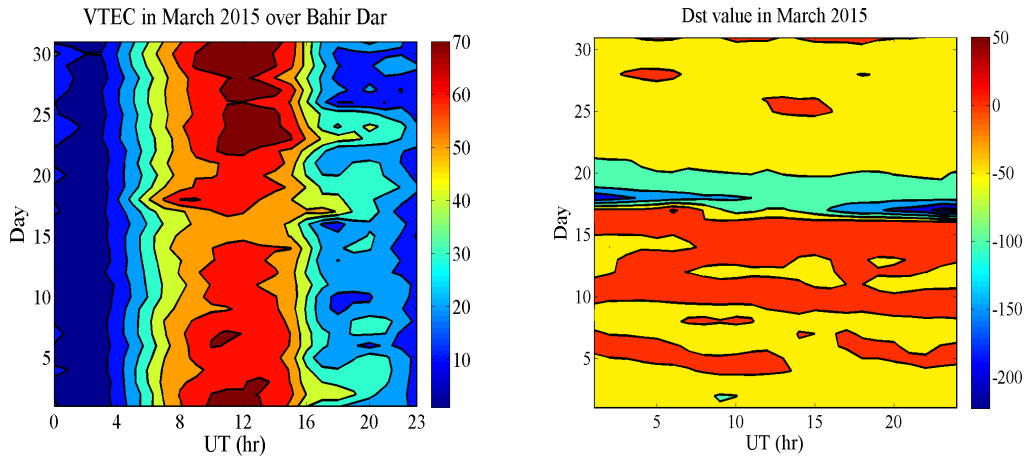

Figure 5.21: Diurnal variation of TEC and Dst value at Bahir Dar Station in March, 2015.

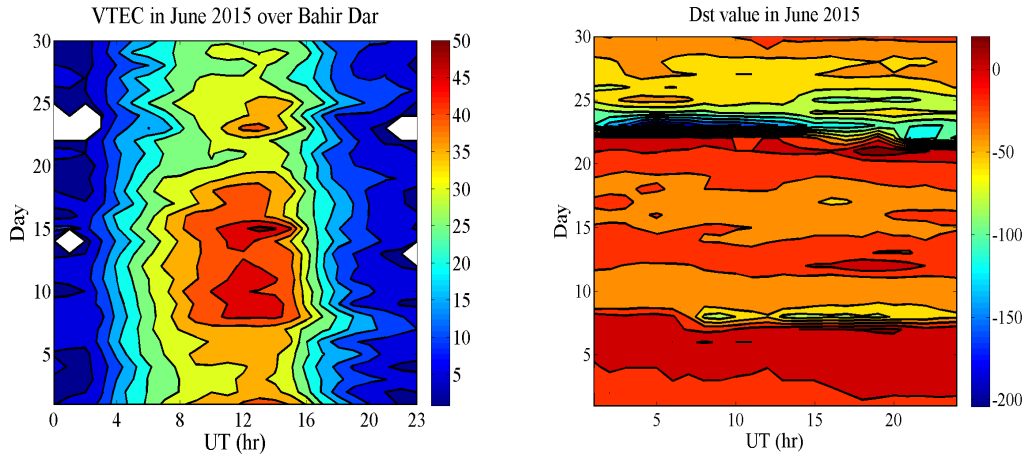

Figure 5.22: Diurnal variation of TEC and Dst value at Bahir Dar Station in June, 2015.

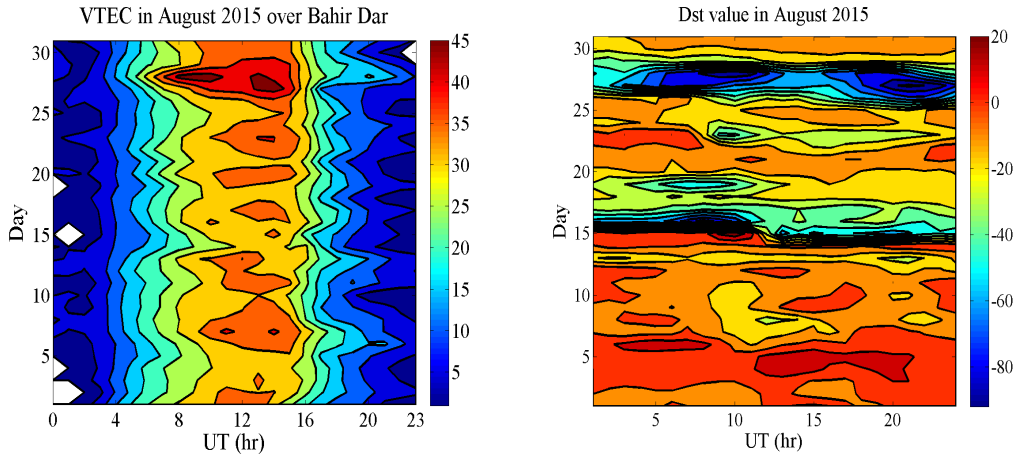

Figure 5.23: Diurnal variation of TEC and Dst value at Bahir Dar Station in August, 2015.

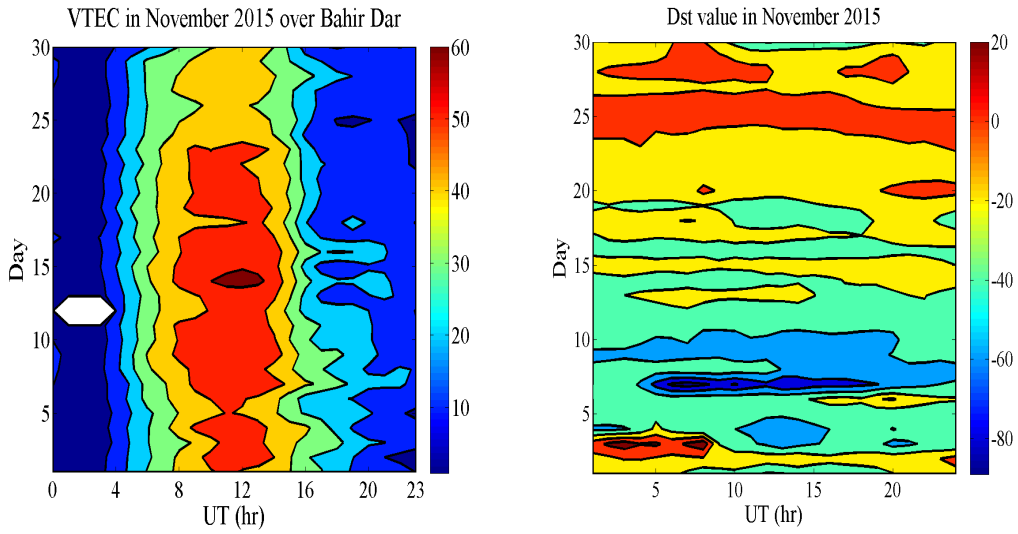

Figure 5.24: Diurnal variation of TEC and Dst value at Bahir Dar Station in November, 2015.

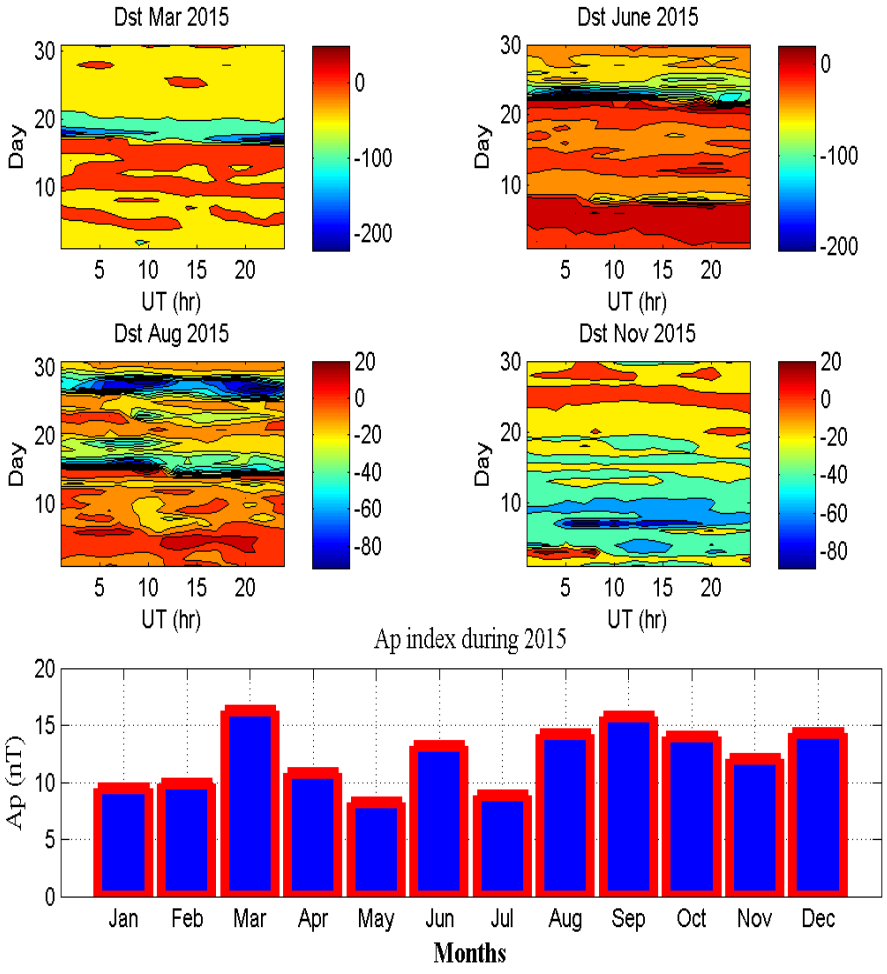

Figure 5.25: Dst index during March, June, August and November and the corresponding Ap index during 2015.

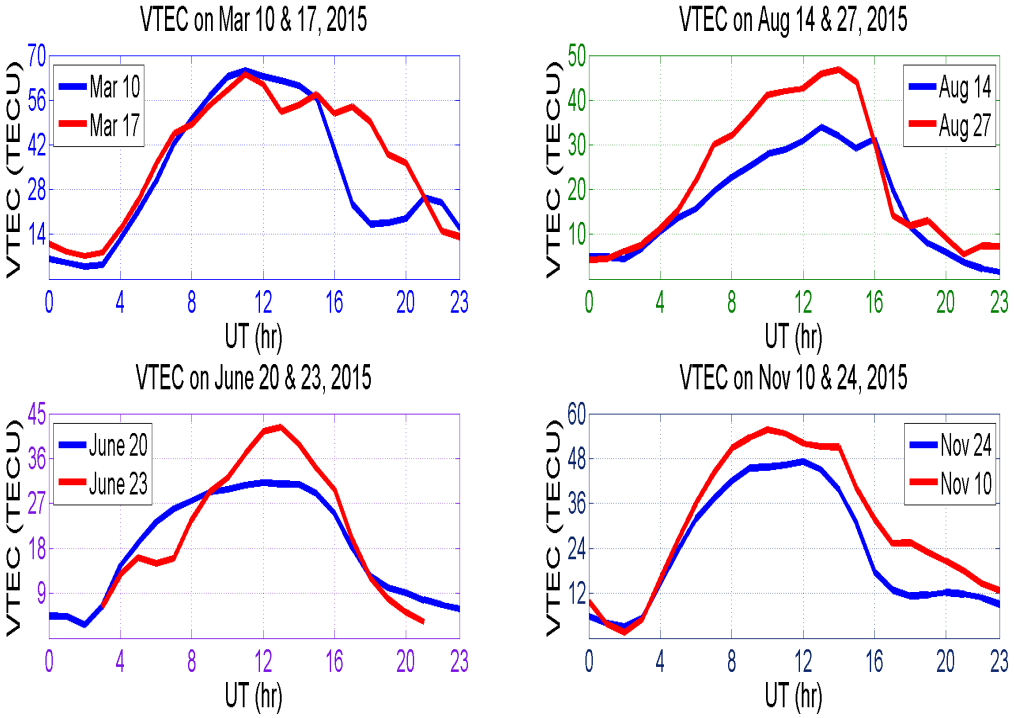

Figure 5.26: TEC values during disturbed and undisturbed days at Bahir Dar, Ethiopia during 2015.

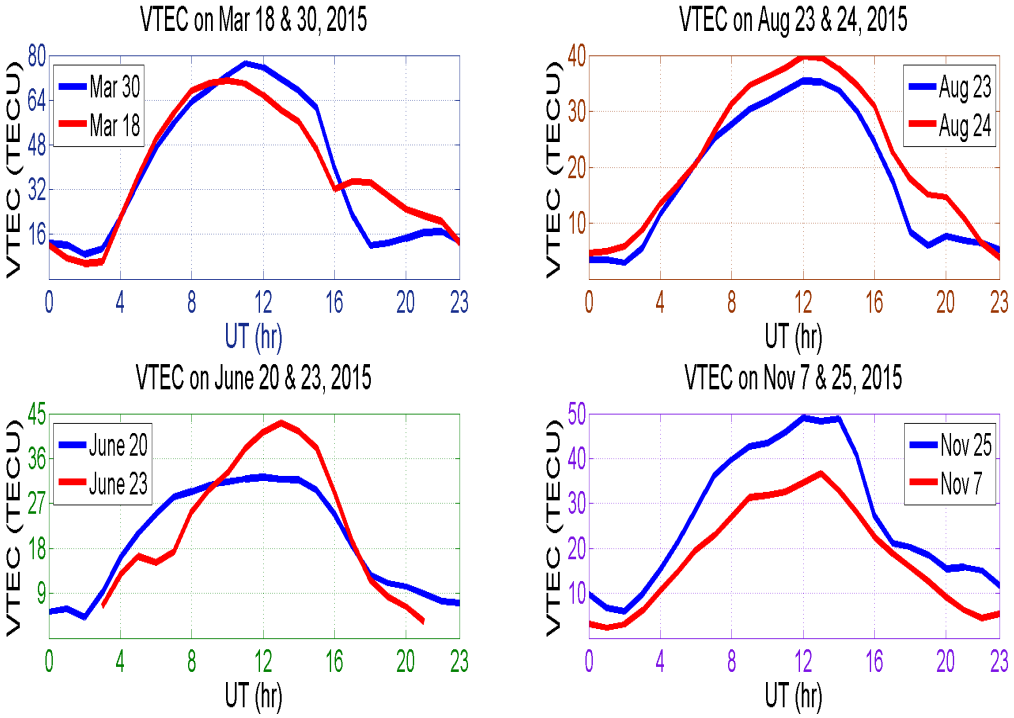

Figure 5.27: TEC values during disturbed and undisturbed days at Addis Ababa, Ethiopia during 2015.

Chapter 6

Conclusions and Recommendations

6.1 Conclusions

From the analysis of TEC values measured by two independent GPS receivers situated at a distance of around 500 km apart and very close to the geographic equator in Ethiopia, East Africa during the year 2015, around peak of solar cycle 24 we found the following.

We made a hourly contour plots of each month, and grouped months into seasons. The results show that the median TEC varies from a pre dawn minimum to an afternoon maximum and then decreases. The daily variation of ionospheric TEC is maximum on the equinoctial and winter days while minimum in summer in both stations.

In all the results obtained the diurnal variations show a maximum occurring of TEC between $0900 - 1500$ UT and short-lived minimum in TEC occurring between $1600-0700$ UT. During February, March and April 2015 the magnitude of the TEC is better than the rest days of other months at $0000 - 2300$ UT. The three months

(March, April and February) TEC value during 2015 at both stations is extremely differ from other months TEC value.

The value of TEC is maximum during the equinoctial and winter seasons as compared to summer season. In the whole seasons the maximum value of TEC leads first in Addis Ababa followed by Bahir Dar. The difference in VTEC over Addis Ababa and Bahir Dar is to the difference in geographical latitude.

The value of TEC increases and decreases in line with the values of solar activity parameters (sunspot number and solar radio flux). We deduce that, during the period of low or high sunspot number and solar radio flux, the provided GPS ionospheric TEC builds up slowly or quickly.

Geomagnetic storm have occurred on June 23, 2015. The Dst values for the day shows that it is an intense intensity geomagnetic storm. The $SYM - H$ value before June 23 shows a sudden increase to more than 50 nT at the sudden storm commencements (SSC)s and then sharp decrease to a value of -204 nT after which a recovering starts followed by another shock on this day. These SSCs before the main storm on June 23 and other indicators are evidences for the occurrence of Coronal Mass Ejection (CME) which causes compression of the magnetosphere leading to fluctuation of the Earth's magnetic field.

We observe that the value of TEC is greater during disturbed days than undisturbed once. In a different case the value of TEC is maximum on undisturbed days of March $17-18$ and November 25, 2015 as compared to disturbed days. The storms occurred during March $17-18$ and November 25 are negative storms while the rest days of geomagnetic storms are positive storms since they increase the value of TEC as compared to other undisturbed days of the observed months. The TEC depletion

on disturbed days may be due to thermosphere composition changes.

In all aspects of observation we saw that the variation of TEC of the ionosphere results due to space weather effects. When TEC is maximized/minimized by storms in the ionosphere the radio communication will also be disrupted.

6.2 Recommendations

Since this study has not covered the whole Ethiopian ionospheric TEC variation we recommend that studies should better to take in all satellite receiver stations in the country first and provide the study in East African countries second since the technology is not yet grow on these sectors.

Bibliography

[1] N. Jakowski, S. Heise, S. Wehrenpfenning, S. Schluter, and R. Reimer. Gps/glonass-based tec measurments as a contribution for space wether forecast. *Atmos. and Sol. Terr. phys*, (64):729–735, 2002.

[2] J. K. Hargreaves. *The solar-terrestrial environment: An introductory to geospace-the science of the terrestrial upper atmosphere, ionosphere and magnetosphere.* Cambridge University Press, New York, 1992.

[3] M. Moldwin. *An introduction to space weather.* Cambridge University Press, New York, 2008.

[4] M. H. Denton, J. E. Borovsky, R. M. Skoug, M. F. Thomsen, B. Lavraud, M. G. Henderson, R. L. McPherron, J. C. Zhang, and M. W. Liemohn. Geomagnetic storms driven by ICME- and CIR-dominated solar wind. *Geophys. Res.*, 111:A07S07, doi:10.1029/2005JA011436, 2006.

[5] J. K. Hargreaves. *The high-latitude ionosphere and its effects on radio propagation.* Cambridge University Press., (2003).

[6] K. Davies. *Ionospheric Radio.* Peter Peregrinus Ltd, London (UK), (1990).

[7] F. N. Okeke and Y. Hamano. Daily variations of geomagnetic H D and Z-fields at equatorial latitudes. *Earth Planets Space*, 52:237–243, 2000.

[8] M. C. Kelly. *The Earth's Ionosphere, plasma physics and electrodynamics*. Academic press, INC, New York, 1989.

[9] B. T. Tsurutani. Solar/interplanetary plasma phenomena causing geomagnetic activity at earth. *IOS Press.*, 273, 2000.

[10] YU You, WAN Wei-Xing, L. Li-Bo, and Z. Bi-Qiang. A global ionospheric tec perturbation index, china. 2009.

[11] P. Song, H. J. Singer, and G. L. Siscoe. Space weather. *AGU Monograph*, 125, 2001.

[12] T. Pulkkinen. Space weather: Terrestrial perspective. *Solar Phys.*, 2007.

[13] L. Rastatter, A. Kuznetsova, M. M. D. Glocer, X. Welling, J. Meng, M. Raeder, Y. Yu Jordanova V. K. Wiltberger, S. R. S. Zaharia, S. Weigel, R. Sazykin, H. Boynton, V. Wei, W. Eccles, Horton, M. L. Mays, and J. Gannon. Geospace environment modeling 2008-2009 challenge: Dst index, spaceweather. 11, 2013.

[14] C. K. Michael. The earths ionosphere plasma physics and electrodynamics. *International Geophysics Series, Academic Press,inc.*, 2009.

[15] S. J. Adolph. *Handbook Of Geophysics and the Space Environment*. United States, 1985.

[16] A. Coster and A. Komjathy. Space weather and the global positioning system. (doi:10.1029/2008SW000400), (2008).

[17] G.G. Abraha. *TEC variablity of low latitude ionosphere and role of dynamical coupling: quite and storm characterstics*. PhD thesis, Addis Ababa University, Ethiopia, May 2014.

[18] R. W. Schunk and W. J. Raitt. Atomic nitrogen and oxygen ions in the daytime highlatitude f region. *J. Geophys. Res.*, 1255(85), 1980.

[19] E. N. Parker. *Interplanetary dynamics processes*. Interscience, New York, 1963.

[20] M. V. Alves, E. Echer, and W. D. Gonzalez. Geoeffectiveness of corotating interaction regions as measured by dst index. *Geophys. Res.*, 111(A7), 2006.

[21] T. Bolt. Space weather:its impact on earth and implications for business. Technical report, National Academy of Sciences, 2010.

[22] R.-S. Kim, K.-S. Cho, Y.-J. Moon, Y.-H. Kim, Y. Yi, M. Dryer, S.-C. Bong, and Y.-D. Park. Forecast evaluation of the coronal mass ejection (cme) geoeffectiveness using halo cmes from 1997 to 2003. *Geophys.*, 110(A11104), 2005.

[23] A. M. Rahman, P. K. Manoharan, and S. Umpathy. Propagation characteristics of coronal mass ejections and their effects at the near-earth environment. *Indian J. radio and space Phys.*, 39:276–279, 2010.

[24] N. Gopalswamy. Coronal mass ejections and space weather. *Selected papers from the 2007 Kyoto Symposium*, pages 77–120, 2009.

[25] L. Biermann. *The solar wind and interplanetary media. In Space Astrophys.* Number 150. McGraw-Hill, New York, 1961.

[26] D. John. *Fix Astronomy Journey to the Cosmic Frontier*. University of Iowa, 1999.

[27] W. S. Robert. *Ionospheres*. Cambridge University, 2009.

[28] B. Asgeir. *Physics of the Upper Polar Atmosphere*. White House, 1997.

[29] S. B. Neeraj, P. Seema, P. Bimal, and P. Kavita. Behavior of plasma and field parameters and their relationship with geomagnetic indices during intense geomagnetic storms of solar cycle 23, india.

[30] J. W. Scott. *Modelling the Temporal Variation of the Ionosphere in a Network-RTK Environment.* Australia, June 2007.

[31] S. F. Rufus, B. Rabiu, O. Olakunle, and G. Keith. Variation of total electron content TEC and their effect on GNSS over Akure, Nigeria. (2012),.

[32] J. LIU, B. Zhao, and L. LIU. *Time Delay and Duration of Ionospheric Total Electron Content Responses to Geomagnetic Disturbances.* Beijing China, march 2010.

[33] M. Das Rupesh, Y. Sneha, R. S. Dabas, S. Shailendra, and A. K. Gwal. *Investigation of TEC Variation and Ionospheric Scintillation at the Two Hemispheres over the Polar Region Using GPS Measurements.* India, (2011).

[34] B. G. Fejer and L. Scherlies. Time dependent response of equatorial ionospheric electric fields to magnetospheric disturbances. *Geophys. Res. lett.*, 22:851, 1995.

[35] L. Schlerliess and B. G. Fejer. Storm-time dependence of equatorial disturbance dynamo zonal electric fields. *J. Geophys. Res.*, 102:24037–24046, 1997.

[36] R. Schunk and A. Nagy. *Ionospheres Physics, Plasma physics, and Chemistry.* Cambridge University press, New York, 2009.

[37] D. Elliott, Kaplan, and Christopher J. Hegarty. *Understanding GPS Principles and Applications.* Artecht House Inc, 2nd edition, 2006.

[38] B. Soumi, PK Purohit, and AK Gwal. *Ionospheric Time Delay Variations in the Equatorial Anomaly Region During Low Solar Activity Using GPS.* India, 2008.

[39] T. Dautermann and E. Calais. *TEC Data Processing Software.* Purdue University., 2008.

[40] B. Bidaine and R. Warnant. Assessment of the NeQuick model at mid-latitudes using GNSS TEC and ionosonde data. *Adv. space Res.*, 45:11221128, 2010.

[41] E. Yizengaw, E. A. Essex, and R. Bisra. The southern hemisphere and equatorial region ionization response for September 22, 1999 severe magnetic storm. *Ann. Geophys.*, 22(8):2765–2773, 2004.

[42] K. Davies. *Ionospheric Radio, radio waves Propagation of effects on ionosphere.* Peter peregrinnes Ltd., Lonodon, United Kingdom, 1989.

[43] N.V. Rao, T. Madhu, and K. L. Kashore. Geomagnetic storm effects on GPS aided Navigation over low latitude south indian region. *Com. sci. and Net. Security*, 10:2765–2773, 2010.

[44] Z. Li, F. Wei, X. Feng, J. Guo, B. A. Emery, and X. Zhao. Large ionospheric disturbances during a minor geomagnetic storm on june 23, 2000. *Ann. Geophys.*, 55:2, doi: 10.4401/ag–5409, 2012.

[45] N. Maruyama, S. Watanabe, and T. J. Fuller-Rowell. Dynamic and energetic coupling in the equatorial ionopsphere and theremosphere. *J. Geophys. res.*, 108:A11, 1396, doi:10.1029/2002JA009599, 2003.

[46] M. A. Abdu and C. G. M. Brum. Electrodynamics of the vertical coupling processes in the atmosphere-ionosphere system of the low latitude region. *Earth Planets Space*, 61:385–395, 2009.

[47] Rama Rae et al. Electrojet strength and local atmospheric conditions in the thermosphere. 1980.

[48] N. Amensisa, K. Sreenu, D. Baylie, N. Melessew, and A.T. Raghavendra. Reaction of ethiopia ionosphere to sun based movement and geomagnetic storm. *Mod. Chem. and App. Sci.*, 2(4):228–234, 2015.

[49] P. V. S. Rama Rao, S. G. Krishna, K. Niranjan, and D. S. V. V. D. Prasad. Temporal and spatial variations in tec using simultaneous measurements from the

indian gps network of receivers during the low solar activity period of 20042005. *Ann. Geophys.*, (24):32793292.

[50] T. R Tyagi. Electron content and its variation over lindau. *Atmos. Sol-Terr. Phys (UK)*, (36):475–487, 1974.

[51] A. B. Rabiu, A. I. Mamukuyomi, and E. O. Joshua. Variability of equatorial ionosphere inferred from geomagnetic field measurements. *Bull. Astr. Soc. India*, 35:607–618, 2007.

[52] R. G. Rastogi, H. Chandra, and M. E. James. Characteristics of equatorial electrojet current in the central regions of South America. *Earth Planets Space*, 60:623–632, 2008.

[53] H. Rishbeth and C. S. G. K. Setty. The F-layer at sunrise. *J. Atmos. Terr.Phys.*, 20(263), 1961.

[54] H. Arnold. *The Sun and Space Weather*, volume 347. 2nd edition, 2007.

[55] G. Jee, R. W. Schunk, and I. Scherliess. Comparison f iri-2001 with topex tec measurments. *Sol. Terr. phys.*, (67):365–380, 2005.

[56] J. H. Sastri. Equatorial Ionosphere-Thermosphere System During Geomagnetic Storms. *Geophysical mongraph series.*, 142:185–203, 10.1029/142GM16, 2003.

[57] B. T. Tsurutani, A. Mannucci, B. Iijima, M. A. Abdu, J. H. A. Sobral, W. Gonzalez, F. Guarneri, and T. Tsuda. Global dayside ionospheric uplift and enhancement associated with in terplanetary electric fields. *Geophys. Res.*, 109:A08302, doi:10.1029/2003JA010342, 2004.

[58] M. A Abdu, J.W.MacDougall, I.S. Batista, J. H. A. Sobral, and P. T. Jayachandran. Equatorial evening prereversal electric field enhancement and sporadic E

layer disruption. A manifestation of E and F region coupling. *J. Geophys. Res.*, 108:A6, 1254, doi:10,1029/2002JA009285, 2003.

[59] J. Guo, X. Feng, P. Zuo, J. Zhang, Y. Wei, and Q. Zong. Interplanetary drivers of ionospheric prompt penetration electric fields. *J. Atmos. Sol. Terr. Phys.*, 73:130–136, 2011.

[60] A.S. Pavlov, S. Fukao, and S. Kawamura. F -region ionospheric perturbations in the low-latitude ionosphere during the geomagnetic storm of 25-27 August 1987. *Ann. Geophys.*, 22:3479–3501, SRef–ID: 1432–0576/ag/2004–22–3479, 2004.

[61] G.M. Lindsay, C.T. Russell, and J. G. Luhmann. Coronal mass ejection and steam interaction region characteristics and their potential geomagnetic effectiveness. *J. Geophys. Res.*, 100:A9, 16999–17013, 1995.

[62] C. V Sreehari and S. R. P. Nayar. Penetration of interplanetary electric field to the equatorial F region during the magnetic storm on November 20, 2003. *ILWS Workshop*, pages GOA 19–24, 2006.

[63] S. Bassiri and G. A. Hajj. Higher order ionospheric effects on the global positioning system observables and means of modeling them. *Manuscripts geodactica*, (18):280–289, 1993.

[64] S. E MacDonald, C. Coker, K. F. Dymond, D. N. Anderson, and E.A. Araujo-Pradere. A study of the strong linear relationship between the equatorial ionization anomaly and the prereversal $E \times B$ drift velocity at solar minimum. *Radio Science*, 46:RS6004, doi: 10.1029/2011RS004702, 2011.